

Dual Pore Network Model of Electrical Resistivity for Carbonate Rocks

by

Donya Ahmadi

A thesis
presented to the University of Waterloo
in fulfillment of the
thesis requirement for the degree of
Master of Applied Science
in
Chemical Engineering

Waterloo, Ontario, Canada, 2014

©DonyaAhmadi 2014

I hereby declare that I am the sole author of this thesis. This is a true copy of the thesis, including any required final revisions, as accepted by my examiners.

I understand that my thesis may be made electronically available to the public.

Abstract

Extreme variability of carbonate depositional environments and susceptibility of carbonate sediments to a host of post-depositional (diagenetic) processes involving mineral dissolution and precipitation, result in complex pore structures comprising length scales from less than a micron and up to several millimeters in the form of vugs and solution channels of varying degree of connectedness. Significant deviations from Archie's law relating the average water saturation to the average electrical resistivity are observed in carbonates. This behavior is a direct, but difficult to interpret or predict, consequence of the complexity of their microstructure. Considering that carbonate reservoirs hold a large fraction of the remaining world oil resources, the need to develop and validate efficient models of carbonate rock resistivity is pressing.

There is now mounting consensus that interpretation of the petro-physical properties of carbonate rocks requires the consideration of dual pore network models (D-PNM). In this context, non- Archie behavior in carbonate rocks is qualitatively related to the degree of connectedness (percolation) of different water fractions, namely water residing in networks comprising pores of significantly disparate scales (micro-porosity and macro-porosity). What is presently lacking is a flexible D-PNM that could be calibrated to core laboratory data (micro-tomography, capillary pressure and resistivity). Availability of such a model would represent a useful advance in the practice of resistivity log interpretation for carbonate reservoirs. To this end, we investigate here a previously reported D-PNM which allows for heterogeneous matrix (micro-porosity) properties and variably-connected macro-porosity. By varying the relative amounts, geometric properties and degree of connectedness of micro-porosity and macro-porosity, we are able to stylistically reproduce all documented deviations of the resistivity index from Archie behavior.

Acknowledgements

First and foremost, I would like to express my sincere gratitude to my supervisor Professor Marios Ioannidis, who has endlessly encouraged, guided and supported me throughout my graduate study. I am deeply grateful for the constant reviews and supervision.

I would also like to convey my gratitude to Professor Ali Elkamel and Professor Yuri Leonenko for giving me necessary advices and precious guidance.

Furthermore, I would like to thank Ms. Judy Caron, administrative co-ordinator of Graduate Studies, for her generous support throughout the entire process.

Also, I would like thank my friends: Navid, Saeed, Sheida, Atoosa, Soosan, Hasan and many others for their encouragements and love through these all years.

Last but not the least, this thesis would not have been possible without the unconditional love and support of my family. My parents: Simin and Masoud, for always being there for me and giving me life's real education. And my siblings: Lena, Amir and Mohammad, who have done everything for me. Thanks for being the best family anybody could ask for.

Dedication

To my supervisor professor Marios Ioannidis who has given me a chance to peruse my dreams by his support, guidance and belief in me.

Table of Contents

List of Figures	viii
List of Tables	x
Chapter 1 Introduction	1
1.1 Carbonate Rocks	1
1.1.1 Motivation.....	1
Non-Archie Behavior of Carbonate Rocks	3
1.2 Objectives	7
Chapter 2 Background	9
2.1 Pore Structure Parameters.....	9
2.1.1 Porosity of Reservoir Rocks	9
2.1.2 Permeability of the Porous Media.....	9
2.1.3 Capillary Properties.....	10
2.1.4 Electrical Properties	13
Chapter 3 Dual Pore Network Model	14
3.1 Model Development.....	14
3.1.1 Geometry of the Dual Pore Network Model.....	14
3.1.2 Assignment of Cell Properties	15
3.1.3 Connectivity and Percolation in the D-PNM	16
Figure 3-3:Cartoon representation of DPNM with 10x10 cells: (a) Percolating vugs in percolating matrix; (b) Percolating vugs in non-percolating matrix; (c) Non-percolating vugs in percolating matrix.	18
3.2 Computation of Drainage Capillary Pressure Curve.....	18
3.2.1 Cell Accessibility to Invading Non-wetting Phase	18
3.2.2 Fluid Saturation Calculations.....	29
3.3 Computation of Resistivity Index	33
3.3.1 Resistivity of a Single Cell.....	33
3.4 Computation of Formation Factor.....	38
Chapter 4 Results and Discussion.....	39
4.1 Model Response.....	39
4.1.1 Single Cell Response	39

4.1.2 Total Network Model Response	41
4.2 Verification of the Model	50
4.2.1 Lavoux Carbonate Sample Verification	52
4.2.2 Estailades Carbonate Sample	54
4.2.3 Parametric Study	56
Chapter 5 Conclusions	61
Chapter 6 Recommendations	63
Bibliograpy.....	84

List of Figures

Figure 1-1: Distribution of carbonate reservoirs worldwide [1].....	1
Figure 1-2: Example of well logging record [1]	2
Figure 1-3: Non-Archie behavior of carbonate rocks [6]	4
Figure 2-1: Mercury capillary pressure curve.....	11
Figure 3-1: A cubic cell as the basic building block of a dual pore network model.	15
Figure 3-2: Secondary porosity distribution: (a) with scale parameter of 0.15 and shape parameter of 1; (b) with scale parameter of 0.17 and shape parameter of 2.	16
Figure 3-3:Cartoon representation of DPNM with 10x10 cells: (a) Percolating vugs in percolating matrix; (b) Percolating vugs in non-percolating matrix; (c) Non-percolating vugs in percolating matrix.	18
Figure 3-4: Hoshen-Kopelman Cluster multiple labeling technique.	20
Figure 3-5: Hoshen-Kopelman data structure.....	20
Figure 3-6: HK cell neighboring cells	21
Figure 3-7: Flow chart of classical HK algorithm	22
Figure 3-8: Csize procedure in HK algorithm	25
Figure 3-9: Connectivity between neighboring cells	27
Figure 3-10: nearest three neighbors.....	28
Figure 3-11: Work flow of the model to find the accessible cluster through the inlet surface	29
Figure 3-12: (a) Half-cell resistivity along one direction considering; (b) conduction through matrix in parallel with conduction through secondary pores.	34
Figure 3-13: Single cell represented in 3D by six identical resistors.	36
Figure 3-14: Calculation of equivalent resistivity of eight neighboring cells	37
Figure 3-15: Schematic of renormalizing 4x4x4 cells to one cell	37
Figure 4-1: Single cell model response: (a) resistivity index vs. saturation, (b) pore entry diameter distribution.....	40
Figure 4-2: DPNM with 10x10 cells.....	41
Figure 4-3: Electrical resistivity and capillary pressure properties of the matrix.....	42
Figure 4-4: DPNM with percolating matrix and percolating vugs.	44

Figure 4-5: Typical response of the PM-PV class of D-PNM	45
Figure 4-6: DPNM with non-percolating matrix and percolating vugs	47
Figure 4-7: Typical response of NPM-PV class of D-PNM.	48
Figure 4-8: DPNM with percolating matrix and non-percolating vugs	49
Figure 4-9: Model response of PM-NPV type	50
Figure 4-10: The SEM image of Lavoux(left) and Estailade Limestone (right) [17].....	51
Figure 4-11: Vug distribution for Lavoux sample	53
Figure 4-12: Lavoux carbonate sample: (a) resistivity index vs. saturation, (b) pore entry diameter distribution.....	54
Figure 4-13: Vug distribution for Estailades sample	55
Figure 4-14: Estailades carbonate sample: (a) resistivity index vs. saturation, (b) pore entry diameter distribution.....	56
Figure 4-15: Effect of zero matrix porosity fractions	57
Figure 4-16: Effect of size ratio R	58
Figure 4-17: Effect of connectivity exponent	59
Figure 4-18: Effect of the shape of vug size distribution.....	60

List of Tables

Table 4-1: Single cell parameters	39
Table 4-2: PM-PV parameters	44
Table 4-3: NPM-PV parameters	46
Table 4-4: PM-NPV parameters	49
Table 4-5: Porosity and formation factor of real samples and DPNM	51
Table 4-6: DPNM parameters	52

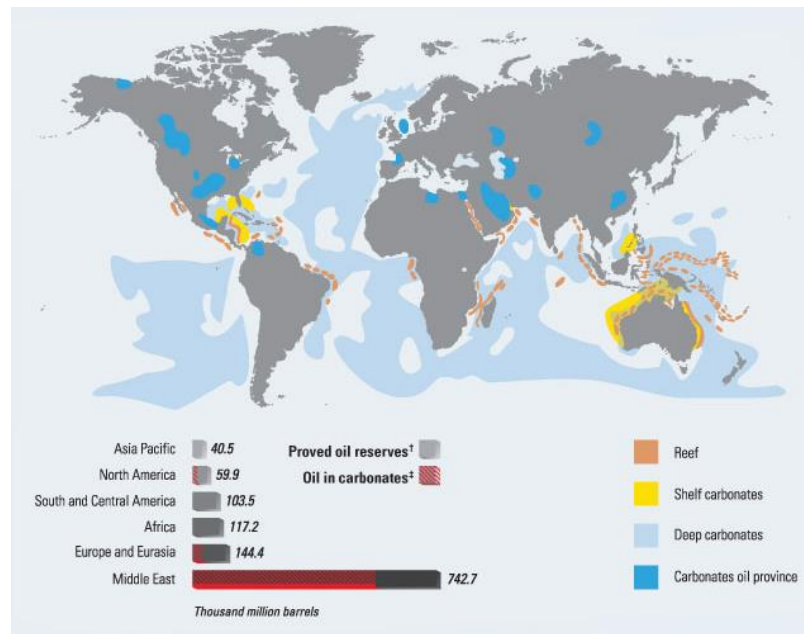
Chapter 1

Introduction

1.1 Carbonate Rocks

1.1.1 Motivation

Statistics demonstrate that the energy consumption has increased significantly in recent years. Prediction confirms the energy demand could surge by 53% until 2030. Fossil fuels are the source of more than 85% of world energy consumption. In addition, more than half of the world's remaining oil and gas is located in carbonate reservoirs. For example, in the Middle East, around seventy percent of oil and ninety percent of gas reserves are held in carbonate reservoirs [1]. Figure 1-1 illustrates the distribution of oil from carbonate reserves around the world.



Distribution of oil from carbonate sources around the world.

Figure 1-1: Distribution of carbonate reservoirs worldwide [1]

In the petroleum industry, logging techniques are applied to obtain a continuous record of the petro-physical properties of reservoir rock by lowering a variety of probes into the borehole. Interpretation of logging tool measurements determines valuable information about the existence and volume of hydrocarbon reserves. Figure 1-2 shows a sample logging record combining traces from three different logging tools. The formation resistivity response of the rock is observed in the second column of Figure 1-2.

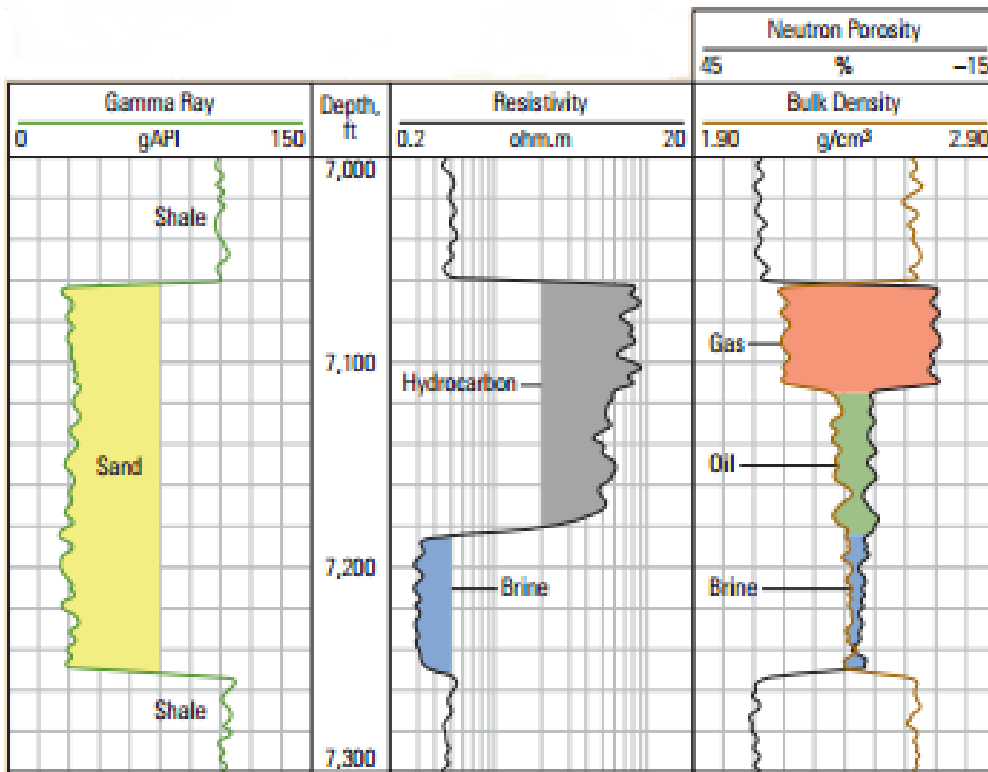


Figure 1-2: Example of well logging record [1]

Formation resistivity is of paramount importance for the determination of hydrocarbon reserves. Consider, for example, the traces shown in Figure 1-2. Whereas other logs (neutron, density, gamma-ray) can identify lithology (sandstone vs. shale), quantify porosity and distinguish gas from liquid (oil and brine), it is interpretation of the resistivity log that enables detection of reservoir zones containing significant amounts of oil. Such interpretation has been traditionally based on Archie's laws, which relate the electrical

resistivity of reservoir rock to water saturation, S_w . These laws, which are obeyed by clean water-wet sandstones [2] are stated below:

$$RI = \frac{R_t}{R_0} = S_w^{-n} \quad (1-1)$$

$$F = \frac{R_0}{R_w} = \phi^{-m} \quad (1-2)$$

$$R_t = R_w \phi^{-m} S_w^{-n} \quad (1-3)$$

In the above equations RI is the so-called resistivity index, defined as the ratio of the resistivity of partially water-saturated rock, R_t , to the resistivity of the fully water-saturated rock, R_0 . F is the so-called formation factor, defined as the ratio of the resistivity of the fully water-saturated rock to the resistivity of a volume of brine of identical dimensions, R_w . In Equation 1-3, which is produced by combining Archie's laws, ϕ is the porosity of the rock, m is the cementation exponent and n is the saturation exponent.

Non-Archie Behavior of Carbonate Rocks

Archie relations are often employed with the assumption that cementation and saturation exponents (m and n) would be equal to two, as is typically the case for sandstones and clean rocks. Carbonate rocks, however, exhibit significant deviations from Archie's laws; the cementation and saturation exponent may vary widely from 1.45 to 5.4. Dixon and Marek (1990) reported that saturation exponent could vary to much less than two (1.3 to 1.8) in carbonate reservoir [3], while for various types of carbonates cementation exponent value may range from about 1.5 to 5.4 [4]. Similarly, Saner (1996) measured the cementation factor of eighty different carbonate rocks with three different methods [5]. After employing error analysis on the measured data, he concluded that the Archie cementation factor could not be reliably used to correlate porosity to the resistivity of fully water-saturated carbonate samples.

In carbonates, not only does the cementation exponent, m , deviate from the classical value of two, but also the dependence of resistivity index on water-saturation demonstrates nonlinear trend in log-log scale, contrary to expectation (see equation 1-1). Fleury (2002) presented experimental measurements of non-linear resistivity Index curve for four different carbonate samples using the Fast Resistivity Index Measurement method [6]. In his study, various shapes of resistivity index curves have been observed, particularly at lower values of the water saturation. The saturation exponent varied with saturation from approximately one to three (see Figure 1-3).

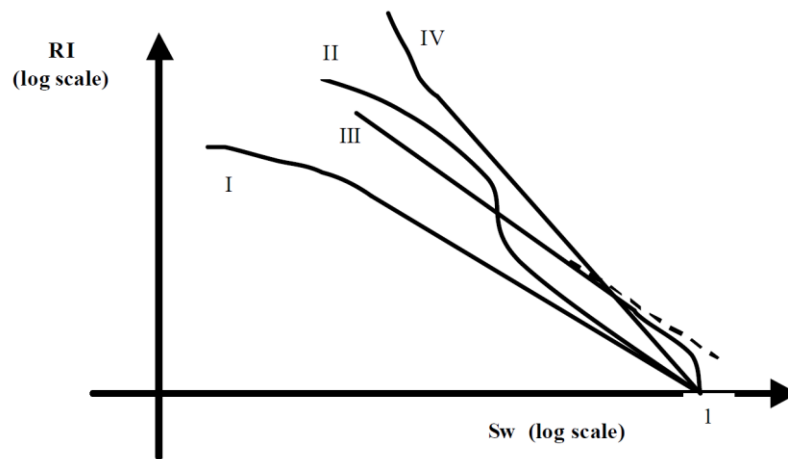


Figure 1-3: Non-Archie behavior of carbonate rocks [6]

In addition, nonlinear behavior of the resistivity index curve has been reported by Padhy *et al.*(2006) for six different carbonate samples. Cementation factors in these samples ranged from 1.99 to 2.68 [7].

The deviations mentioned above are believed to originate from the existence within carbonate rocks of at least two different pore systems at rather disparate length scales, but these deviations have not been completely quantified to date. Petricola and Watfa (1995) considered a dual pore geometry to highlight the significant influence of microporosity on electrical resistivity and the estimation of water saturation thereof [8]. They suggested that the observed low resistivity behavior may be the result current transport along a parallel conduction path formed by water-saturated micropores. They concluded that two

parameters are essential for the modeling of carbonate rocks with heterogeneous structure: the amount and the distribution of micro-porosity relative to macroporosity. In their view, the first step for solving this problem was the measurement of the pore size distribution of carbonate rocks. They presented a saturation equation to consider the effect of parallel current-carrying path for two pore size populations (macro and micro). In their equation the conductivity (C) is determined by:

$$C = C_M + C_\mu = C_w (\phi_M^{m_M} S_{wM}^{m_\mu} + \phi_\mu^{m_\mu} S_{w\mu}^{n_\mu}) \quad (1-4)$$

where C_M, C_μ, C_w are the conductivities of vug network, matrix network, and water respectively. ϕ_M is the macro intergranular porosity and ϕ_μ is the micro-porosity. S_w refers to the saturation while m and n are the cementation factor and saturation exponent respectively (including subscripts 'M' for macro-porosity and 'μ' for micro-porosity). It must be noted that while equation (1-4) can be made to fit certain types of non-Archie behavior after adjusting the four exponents, it gives no insight on the way the water saturation of the two different pore populations changes during drainage of the aqueous phase.

Dixon and Marek (1990) studied two different Middle Eastern carbonate samples with low saturation exponent (median of 1.45) using Scanning Electron Microscopy and high pressure mercury porosimetry. Two pore size populations (inter-particle macro-pores and inter-particle micro-pores) were detected in their experimental study of low resistivity carbonates. They suggested that a network of interconnected micro-pores may be the cause of anomalously low saturation exponents [3]. However, Dicker and Bemelmans (1984) observed that the bending down resistivity behavior at low saturation is strongly depended on thick water layer [9]. This was later confirmed by Han *et al.* (2007) who reported that the low resistivity behavior is due to the existence of a thick water film [10].

On the other hand, Sen (1997) has pointed out the anomalously large resistivity increase as the conducting water phase becomes trapped in isolated regions. He considered three different pore size distribution (micro-porosity, macro-porosity and vugs) and employed effective medium theory to compute the effect of micro-porosity on resistivity [11]. He

indicated that the dependence of electrical resistivity on water saturation is significantly modified when the main current-transporting pathway is changed as a result of desaturation. The effect of secondary porosity on the electrical conductivity of water-saturated carbonates containing both micro-pores and macro-pores (vugs and solution channels) has been analyzed by Ioannidis *and coworkers* (1997) using direct numerical simulation [12]. They proposed that the cementation exponent in these types of rocks is related to the spatial connectivity of the secondary pore system in addition to the amount of micro-porosity and macro-porosity. More recently, attention was drawn to the effect of percolation of secondary porosity, by Montaron (2009) who interpreted empirically non-Archie resistivity curves using a water connectivity correction index [13].

As mentioned above, most studies conclude that the non-Archie behavior of carbonate rocks is attributed to the geology of heterogeneous porous medium and connectivity of the porosity (percolation). Zou *et al.* (1997) developed a simple bond model to consider the effect of wettability on electrical resistivity of porous media by implementing percolation concepts [14]. They concluded that the simple model is not capable of reproducing the observed deviation and emphasized the need to take into account the effect of water remaining in corners and crevices of otherwise drained pores. Padhy *et al.* (2006) modified the saturation equation proposed by Pericola and Walfra based on connectivity of two pore size populations (micro-pores and macro-pores) and included a layer of water in pore boundaries for a water-wet system [15]. The theoretical resistivity model results compared favorably to the measured experimental one.

Fleury (2002) proposed a double porosity conductivity model (DPC) and triple porosity conductivity model (TPC) to explain the nonlinear behavior in carbonate resistivity curves [6]. The DPC model was employed to reproduce the bending down of RI at low saturations. In this model, two porosity populations are considered in parallel current-carrying paths. The TPC model was implemented to explain the bending up at high and intermediate water saturations and bending down at low saturation. Three different pore size distributions are imagined in the model (micro-pores, meso-pores and macro-pores). Meso-pores and macro-pores are assumed to act electrically in series and the sum of them is in parallel with the

micro-pores. Both models reproduce the bending down shapes due to the electrical parallel path. For the other non-linear shapes, he suggested that the parallel conductivity path should be considered for their modeling.

Han et al. (2007) investigated the effect of continuous thick water films on the electrical resistivity using numerical computation carried out directly on micro-tomographic images from four different groups of sandstones and carbonates [10]. These four different textures are classified based on size, distribution and connectivity of the pores containing both single pore size distribution and bimodal pore size distribution. The authors demonstrated that, at low levels of the water saturation, the electrical behavior is dominated by conduction via continuous water films covering the solid surface, resulting in a significant decrease of the apparent resistivity exponent. Han et al. further proposed that for carbonate samples with a double pore size distribution, the electrical behavior depends strongly on the spatial distribution and connectivity of the micro-porosity [16].

Recently, Bauer *et al.* (2011) reproduced electrical responses of two different carbonates (Estailades and Lavoux carbonates) using a Dual Pore Network Model(D-PNM)parameterized on the basis of extensive analyses of high-resolution micro-tomographic data [17].Their work, which to our knowledge represents the most sophisticated attempt in quantifying the electrical resistivity behavior of carbonates, drew the attention to significant uncertainty owed to the inability of currently available methods to resolve all length scales of relevance to current transport.

1.2 Objectives

With the exception of the work of Bauer *et al.* (2011), the models developed to explain the non-Archie behavior of carbonate rocks are purely empirical. When these models are fitted successfully to experimental data, little insight is provided on the relationship between best-fit parameters and measurable attributes of the microstructure [17]. These models do not resolve carbonate rock microgeometry to any extent beyond asserting volume fractions and cementation and saturation exponents for different pore populations. More importantly, these models make no attempt to quantify the connectivity of different pore populations.

While they aid conceptual understanding, they cannot be informed by petrophysical measurements and are, for this reason, of little predictive value. The work of Bauer *et al.* (2011) on the other hand, has advocated detailed pore network extraction directly from microtomographic data. While x-ray microtomography is common nowadays, pore network extraction is a difficult task fraught by limitations in the ability of presently available instruments to resolve all pore length scales in carbonate rocks.

The main hypothesis of this thesis is that there exists a minimal parametrization of a dual pore network model (D-PNM) that captures most, if not all, features of carbonate rock microstructure that are essential to the quantitative, sample-specific, modeling of electrical resistivity. The model extends of the original work of Ioannidis (1993) (see also [18]) on the capillary properties of heterogeneous carbonate rocks by endowing the D-PNM with the capability to the resistivity index under condition of drainage.

We demonstrate that the model is capable of generating the behavior of electrical resistivity for two different types of carbonates (Estailades and Lavoux carbonates) discussed in the recent literature by Bauer *et al.* (2011) [17] and is consistent with the capillary pressure data. Parametric studies further confirm the model's ability to stylistically reproduce all documented deviations of the resistivity index from Archie behavior [6], suggesting opportunities for rapid assessment via a constrained optimization approach conditioned on micro-tomographic data.

Chapter 2

Background

2.1 Pore Structure Parameters

2.1.1 Porosity of Reservoir Rocks

Porosity is the percentage of bulk rock volumes occupied by pores that is the fraction of void space. This pore volume fraction contains the fluids inside the rock and may change from zero to one. There are two types of porosity. One is porosity which is formed during the rock deposition process, termed primary porosity and porosity that is the result of post-depositional and diagenetic process, termed secondary porosity. Different experimental methods of measuring the porosity have been reviewed in detail by Dullien [19].

The porosity of sandstone may vary between 10% and 30%. In carbonate rocks the porosity varies widely due to numerous diagenetic processes which can reduce or increase the porosity of initial sediments [20]. The primary and secondary porosities are related by the following equation:

$$\phi_v = \frac{\phi_s - \phi_m}{1 - \phi_m} \quad (2-1)$$

where ϕ_v is the secondary porosity (vugs), ϕ_s is the total porosity and ϕ_m is the primary porosity (matrix).

2.1.2 Permeability of the Porous Media

Permeability (k) measures the conductivity of the medium to flow and it is only a function of the geometric and topological characteristics of the porous media. The absolute permeability is described mathematically by Darcy's law:

$$v = -\left(\frac{k}{\mu}\right)(\nabla P - \rho g) \quad (2-2)$$

where v is the named “filter” velocity vector, ∇P is the pressure gradient, μ is the fluid viscosity, ρ is the fluid density and g is the acceleration due to gravity [19].

2.1.3 Capillary Properties

2.1.3.1 Capillary Pressure in Porous media

The existence of surface tension gives rise to a pressure difference across a curved interface separating two immiscible fluids at equilibrium. At equilibrium, the surface tension must be balanced out with a pressure differences, which is described mathematically by Laplace’s equation [21]:

$$P_{nw} - P_w = \frac{2\sigma}{R_m} \quad (2-3)$$

where σ is the surface tension or the interfacial tension, R_m is the mean radius of curvature of the interface and P_{nw} and P_w are pressures of non-wetting and wetting phase respectively.

The mean radius of the curvature of each fluid-fluid interface is a function of the local pore space geometry and the wettability of the solid surface, the latter measured by the contact angle. For capillaries of simple cross-section, the capillary pressure is generally described as:

$$P_{nw} - P_w = \frac{\sigma f(\theta)}{r_c} \quad (2-4)$$

where, r_c is a characteristic pore size and $f(\theta)$ is a function of the contact angle θ formed between two immiscible fluids and the pore wall. Capillary Pressure Curves

Interfacial configurations realized during quasistatic immiscible displacement of one fluid by another in porous media, give rise to a relationship between capillary pressure and wetting

phase saturation – the so-called capillary pressure curve. Capillary pressure curves exhibit hysteresis between drainage (decreasing wetting phase saturation) and imbibition (increasing wetting phase saturation), as shown in Figure 2-1.

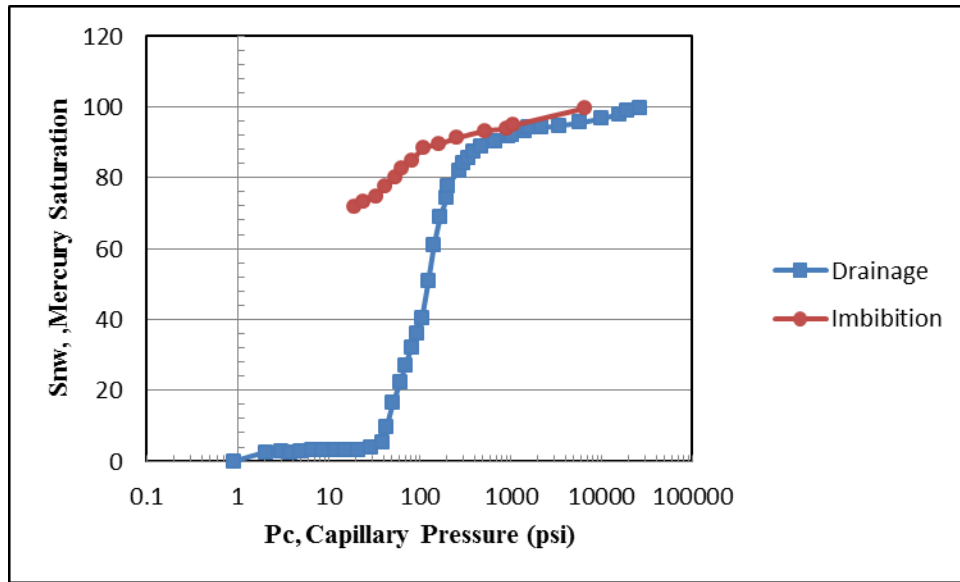


Figure 2-1: Mercury capillary pressure curve

2.1.3.2 Break through Capillary Pressure

During the drainage of a wetting phase by a non-wetting one, a characteristic value of capillary pressure (the breakthrough capillary pressure) is associated with the first formation of a sample-spanning (percolating) connected pathway of pores invaded by the non-wetting phase. The breakthrough pressure can be identified with the inflection point in the drainage capillary pressure curve. Since the connected pathway associated with breakthrough of the non-wetting phase comprises the largest pores, it is not surprising that the breakthrough capillary pressure is strongly correlated with permeability. Such a correlation has been reported by Chatzis (1980) for sandstones [22]:

$$P_c^\circ = 85.63 k^{-0.369} \quad (2-5)$$

where P_c° is the mercury-air capillary pressure in psi and k is the absolute permeability in mDarcy.

Non-wetting phase breakthrough in a network of pores happens as the non-wetting phase invades a number of interconnected pores. The breakthrough capillary pressure or penetration of a non-wetting phase (e.g., air) into a pore throat of rectangular cross-section may be computed by implementing the following approach, originally put forward by [23] for pores of square cross-section, and later extended by Ioannidis (1993) derived the following expression relating the dimensionless capillary pressure as a function of the dimensionless interface radius of curvature [20]:

$$P'_c = \frac{(\lambda + 1) \cos \theta_R + R' F_1(\theta_R)}{\lambda - R'^2 F_2(\theta_R)} \quad (2-6)$$

where,

$$F_1(\theta_R) = \left(\frac{\pi}{2} - 2\theta_R\right) - 2\sqrt{2} \cos \theta_R \sin\left(\frac{\pi}{4} - \theta_R\right) \quad (2-7)$$

$$F_2(\theta_R) = \frac{1}{2} \sin\left(\frac{\pi}{2} - 2\theta_R\right) + \sin^2\left(\frac{\pi}{4} - \theta_R\right) - \left(\frac{\pi}{4} - \theta_R\right) \quad (2-8)$$

$$P'_c = \frac{P_c b}{\sigma} \quad (2-9)$$

$$R' = \frac{R}{b} \quad (2-10)$$

where P'_c and R' are dimensionless capillary pressure and dimensionless radius. P_c is the capillary pressure, b is the side length of the throat, σ is the interfacial tension and R is the interface radius of curvature. The breakthrough capillary pressure that may be realized inside pore throats is the minimum capillary pressure of the interface. Therefore, it is determined by computing the minimum P'_c by employing:

$$\frac{dP'_c}{dR'} = 0 \quad (2-11)$$

By differentiating from equation (2.5), we obtain:

$$R'^2 F_1(\theta_R) F_2(\theta_R) + 2(\lambda + 1) \cos \theta_R F_2(\theta_R) R' + \lambda F_1(\theta_R) = 0 \quad (2-12)$$

After calculating the roots of equation (2-12), the non-negative root R' is substituted in equation (2-5) to determine P_c' . The breakthrough capillary pressure of the throat is then obtained from equation (2-8).

2.1.4 Electrical Properties

The porous media contain solid grains and void spaces which may occupy by fluids. In petroleum reservoirs, mainly the solid and hydrocarbon phases (gas and oil) are non-conductive. The conducting phase of the rock is the water including dissolved salts. Therefore, the electrical properties of the rock depend on the saturation of the conducting fluid and its distribution inside the voids [24].

Chapter 3

Dual Pore Network Model

3.1 Model Development

3.1.1 Geometry of the Dual Pore Network Model

The dual pore network model (DPNM) corresponds to a tessellation of the bulk rock space in cubic cells of side length ℓ . The model is an attempt to provide a minimalist description of carbonate pore space by capitalizing on local porosity information that is nowadays readily available by x-ray microtomography. Such information consists of 3D maps of local porosity, ϕ_s , which may be further differentiated into matrix porosity that is typically below the resolution limit, and resolved secondary or vuggy porosity [17]. Accordingly, each cell comprises a cubic vug (of side length a) connected to six channels with rectangular cross-sections (of side length b , where $R = b/a$). Consider a cubic cell of bulk volume l^3 identified by its spatial location (x, y, z) , as shown in Figure 3-1. The cell contains a vug body of side length $a(x, y, z)$. Connection to vugs in adjacent cells is provided by six throats of side length $b(x, y, z)$ ($0 \leq b(x, y, z) \leq a(x, y, z)$) drilled into each face of the cubic cell towards the central vug. The remainder of the cell volume is occupied by rock matrix of unresolved geometry.

The vuggy porosity (fraction of the cell bulk volume occupied by secondary pores), ϕ_v , is expressed in terms of the side length of the vug body, $a(x, y, z)$, the size of the cubic cell l , and the aspect ratio R as shown below [18].

$$\phi_v(x, y, z) = (1 - 3R^2) \left[\frac{a(x, y, z)}{l} \right]^3 + 3R^3 \left[\frac{a(x, y, z)}{l} \right]^2 \quad (3-1)$$

where,

$$0 \leq a(x, y, z) \leq l$$

$$0 \leq R \leq 1$$

Given ϕ_v , R and l , $a(x,y,z)$ is determined by solving equation (3-1) and $b(x,y,z)$ is computed as R , $a(x,y,z)$.

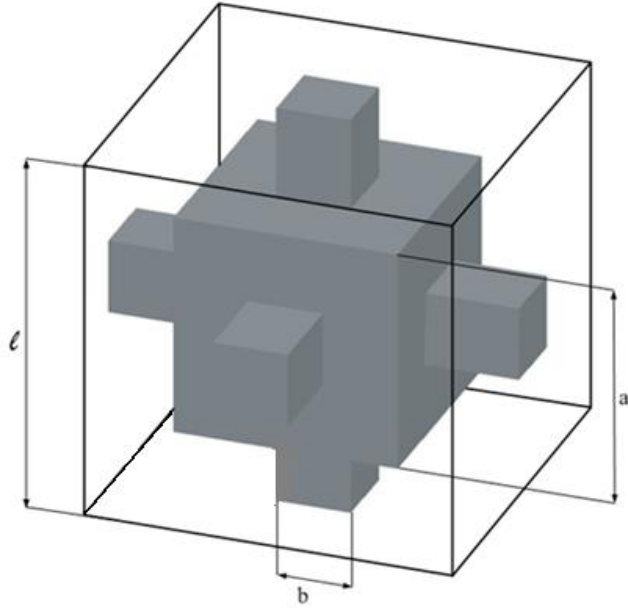


Figure 3-1: A cubic cell as the basic building block of a dual pore network model.

3.1.2 Assignment of Cell Properties

As mentioned before, each cell comprises *geometrically unresolved* porosity (hereafter referred to as matrix) characterized in terms of macroscopic properties (porosity, permeability, capillary pressure, cementation and saturation exponents) which are assumed to be known. Matrix properties may be spatially distributed and/or cross-correlated. Additionally, *geometrically resolved* secondary porosity in the form of a cubic vug and connecting throats is also present. Ideally, $\phi_v(x, y, z)$ is known from 3D microtomographic images. In the absence of such information we assume here that the secondary porosity is a random variable following the Weibull distribution with no spatial correlations. The probability density function of Weibull-distributed random variable x is given by

$$f(x, k, \lambda) = \begin{cases} \frac{k}{\lambda} \left(\frac{x}{\lambda}\right)^{k-1} e^{-(x/\lambda)^k} & x \geq 0 \\ 0 & x \leq 0 \end{cases} \quad (3-2)$$

where k and λ are the shape parameter and scale parameter, respectively. The mean of the distribution is calculated as

$$Mean = \lambda \Gamma\left(1 + \frac{1}{k}\right) \quad (3-3)$$

where Γ is the gamma function. For the same average secondary porosity, very different distributions are obtained by altering the shape and scale parameters, as demonstrated in Figure 3-2 for average vug porosity of 0.15. It is important to remember that the distributions and spatial structure of both matrix and vug porosity are an input to the D-PNM, as this information is experimentally accessible by x-ray microtomography.

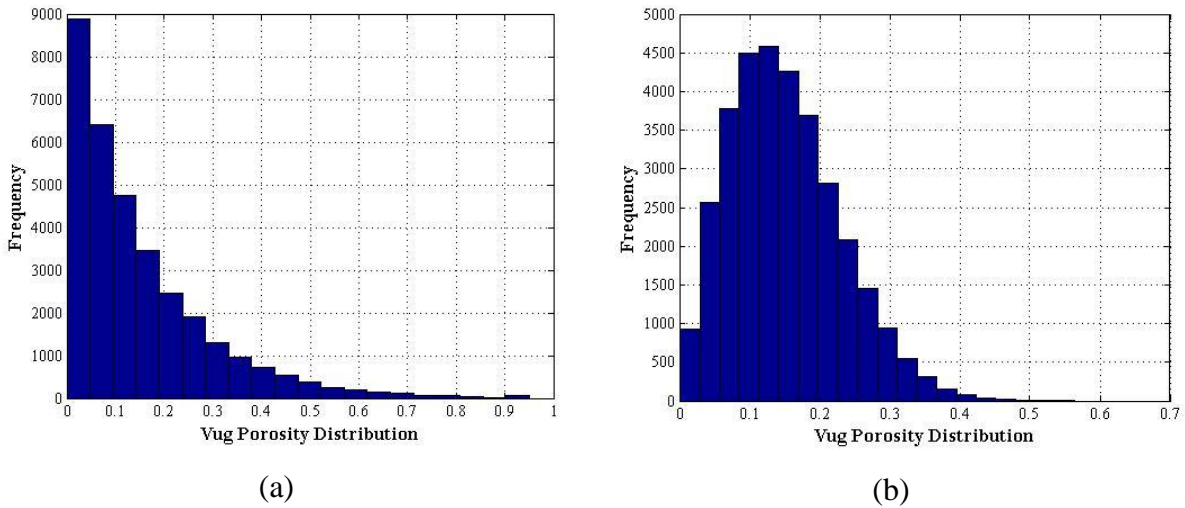


Figure 3-2: Secondary porosity distribution: (a) with scale parameter of 0.15 and shape parameter of 1; (b) with scale parameter of 0.17 and shape parameter of 2.

3.1.3 Connectivity and Percolation in the D-PNM

Each cell within the D-PNM may contain both matrix and vuggy porosity. A connected (percolating) path may therefore exist for an invading non-wetting phase to break through the

entire pore network via matrix pores, secondary pores (vugs) or a combination of both. The degree of percolation of both matrix and vuggy porosity can be adjusted independently in the DPNM. The percolation of the matrix pore space is modified by designating a fraction f_m^0 of cells to have negligible matrix porosity. Cells with non-zero matrix porosity are assigned a uniform value of matrix porosity, ϕ_m , such that the average matrix porosity of the entire DPNM is $(1 - f_m^0)\phi_m$. In the absence of spatial correlations, $(1 - f_m^0) > 0.32$ ensures percolation of the matrix in 3D (Ioannidis et al, 1993). Figure 3-3 represents a schematic of two-dimensional networks of 10x10 cells in which either one or both matrices and secondary porosities form percolating networks. A D-PNM in which the matrix percolates is shown in Figure 3-3(a) whereas, Figure 3-3(b) illustrates a D-PNM with non-percolating matrix.

Furthermore, the connectivity of the secondary pore space (vugs) may be adjusted to obtain models with varying degrees of percolation of an invading non-wetting phase via secondary pore space. Since each cell containing a cubic vug is also assumed to contain six throats providing communication to secondary pore space in neighboring cells, vug connectivity is adjusted using a probabilistic rule that takes account the amount of vug porosity in adjacent cells. The strength of the probability for a communication to exist between two adjacent cells is controlled by a connectivity exponent (ω) (taking values between zero and one). For two neighboring blocks located at point x and x^* , the probability of finding connection between them ($p(\vec{x}, \vec{x}^*)$) is proportional to the product of local vug porosity values and it can be expressed by equation (3-4) [18]. Figure 3-3(a) and Figure 3-3(c) demonstrate the case where $\omega = 0.9$ and $\omega = 0.2$, leading to the percolating and non-percolating secondary porosity respectively.

$$p(\vec{x}, \vec{x}^*) = [\phi_v(\vec{x}) \cdot \phi_v(\vec{x}^*)]^{1-\omega/\omega} \quad (3-4)$$

where,

$$0 < \omega < 1$$

$$\begin{cases} \text{if } \phi_v(\bar{x}) = 0 \text{ or } \phi_v(\bar{x}^*) = 0 & p(\bar{x}, \bar{x}^*) = 0 \\ \text{if } \phi_v(\bar{x}) = 1 \text{ and } \phi_v(\bar{x}^*) = 1 & p(\bar{x}, \bar{x}^*) = 1 \end{cases}$$

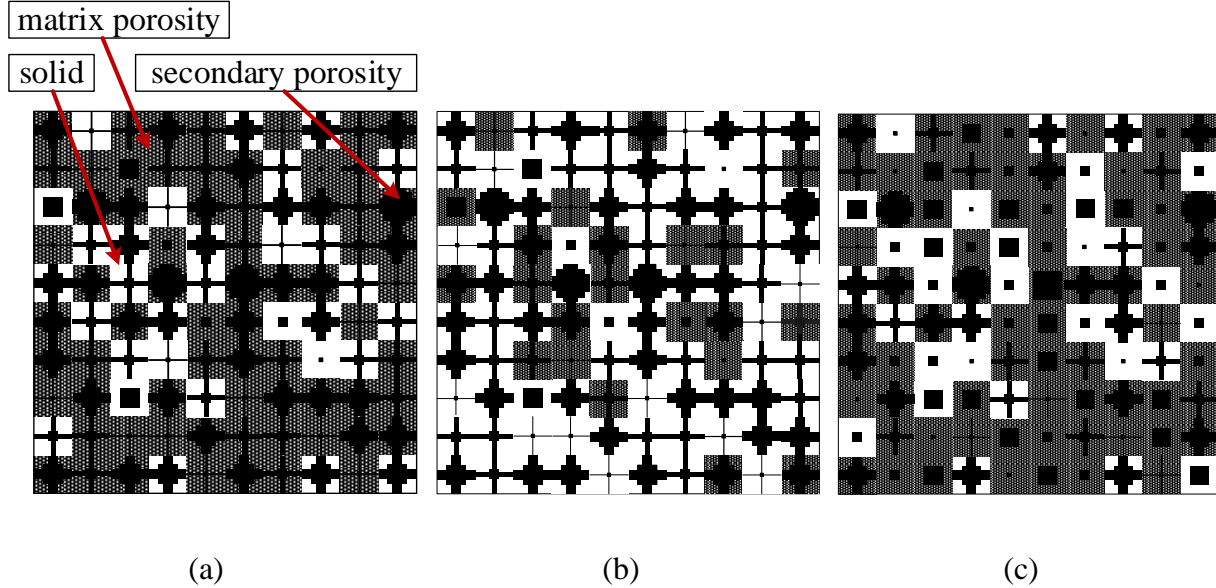


Figure 3-3:Cartoon representation of DPNM with 10x10 cells: (a) Percolating vugs in percolating matrix; (b) Percolating vugs in non-percolating matrix; (c) Non-percolating vugs in percolating matrix.

3.2 Computation of Drainage Capillary Pressure Curve

3.2.1 Cell Accessibility to Invading Non-wetting Phase

In DPNM, each cell may be invaded by a non-wetting phase via matrix or secondary pores according to the rules governing capillarity-dominated displacement. A cluster multiple labeling algorithm is employed to determine the fluid occupancy of matrix and secondary porosity in each cell. This enables the determination of water saturation as a function of increasing capillary pressure.

3.2.1.1 Identification of “Open” cells

The first step in the modeling of capillary pressure versus saturation relationship using the D-PNM is the identification of cells with the potential to be invaded by the invading non-wetting phase, hereafter referred to as “open” cells, at each level of applied capillary pressure. In general, each cell may be penetrated through matrix pore space or vuggy porosity. Penetration of the non-wetting phase into the matrix is limited by the matrix breakthrough capillary pressure, whereas penetration into the secondary pore space is limited by a breakthrough capillary pressure dependent on the size of vug throats. . The calculation of breakthrough capillary pressure of the matrix is explained in section 2.1.3.2. Using the dimensions of cubic vug and connecting throats the breakthrough capillary pressure of the vugs is obtained for each cell as discussed in section 2.1.3.2. The smaller of the two is the capillary pressure at which non-wetting phase first enters the cell (cell breakthrough pressure) as the externally applied capillary pressure is increased in a step-wise fashion. Specifically, at each level of externally applied capillary pressure a cell is marked as “open” if the cell breakthrough pressure is smaller than the externally applied capillary pressure, in the computer program, an array stores binary indicator values where 1 identifies open cells.

3.2.1.2 Clustering of Open Cells

In order to follow the invasion of cells within the D-PNM by a non-wetting phase it is necessary to determine the accessibility of open cells at each level of externally applied capillary pressure. This is so because cells which are open at any given value of capillary pressure may not be part of a cluster of adjacent open cells with a connection to the invasion boundary surface. Clustering of open cells is achieved by an algorithm originally due to Hoshen and Kopelman [25] after some modifications as explained next.

The original 2-dimensional Hoshen-Kopelman algorithm assigns unique labels to distinct clusters of occupied or unoccupied cells on a grid. Figure 3-4 demonstrates the cluster labeling for an occupied (indicator value of one) cells in a hypothetical matrix. Assuming 4-neighbor adjacency, the presence of five different clusters is detected by the HK algorithm. Cells belonging to the same cluster share the same cluster label.

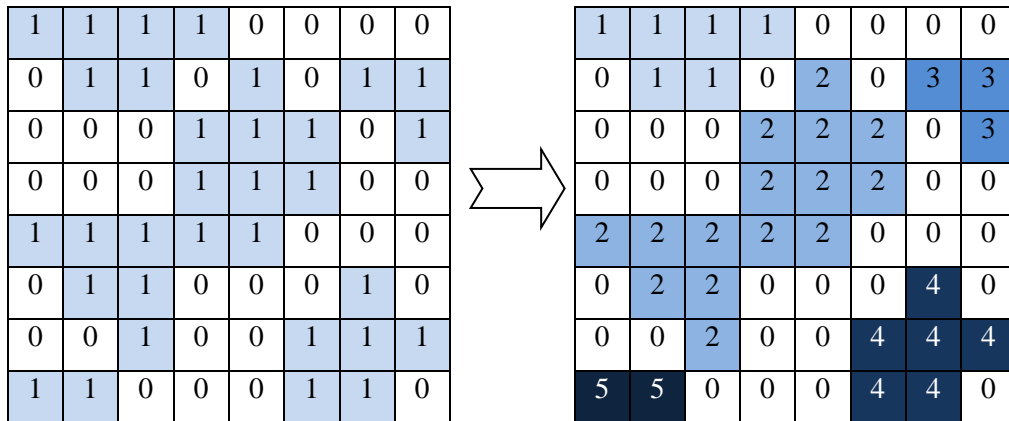


Figure 3-4: Hoshen-Kopelman Cluster multiple labeling technique.

The basic 2-D HK algorithm has two data structures serving the following functions [26].

1. The working matrix
 - Stores occupied (indicator value of one) and unoccupied (indicator value of zero) cells.
2. Cluster label Array (Csize)
 - Counts the cluster labels.
 - Can have positive or negative value.

Figure 3-5 illustrates the HK matrix and Csize array data structures

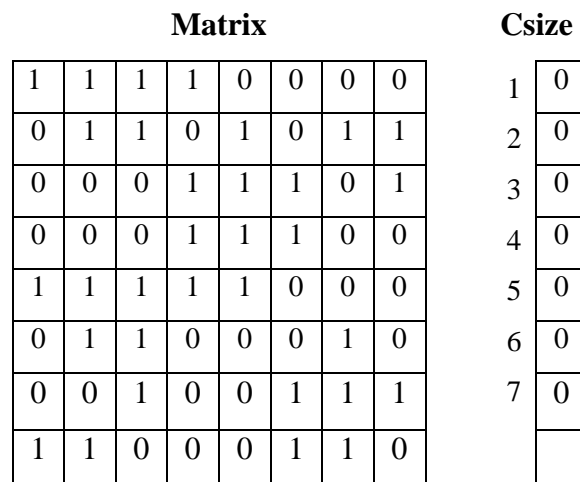


Figure 3-5: Hoshen-Kopelman data structure

Matrix Procedure: The matrix is traversed row-wise to identify members of same cluster by checking its four neighbors as demonstrated in Figure 3-6. Each cell's attribute ("open" or not) is checked and if the cell is "open", it is assigned the same cluster label as the neighbor's label. The Csize array is changed as will be described below). If no neighbor from which to inherit a cluster label is found, then a new cluster label is assigned to the cell. Figure 3-7 is a flow chart of the matrix traversing procedure [25].



Figure 3-6: HK cell neighboring cells

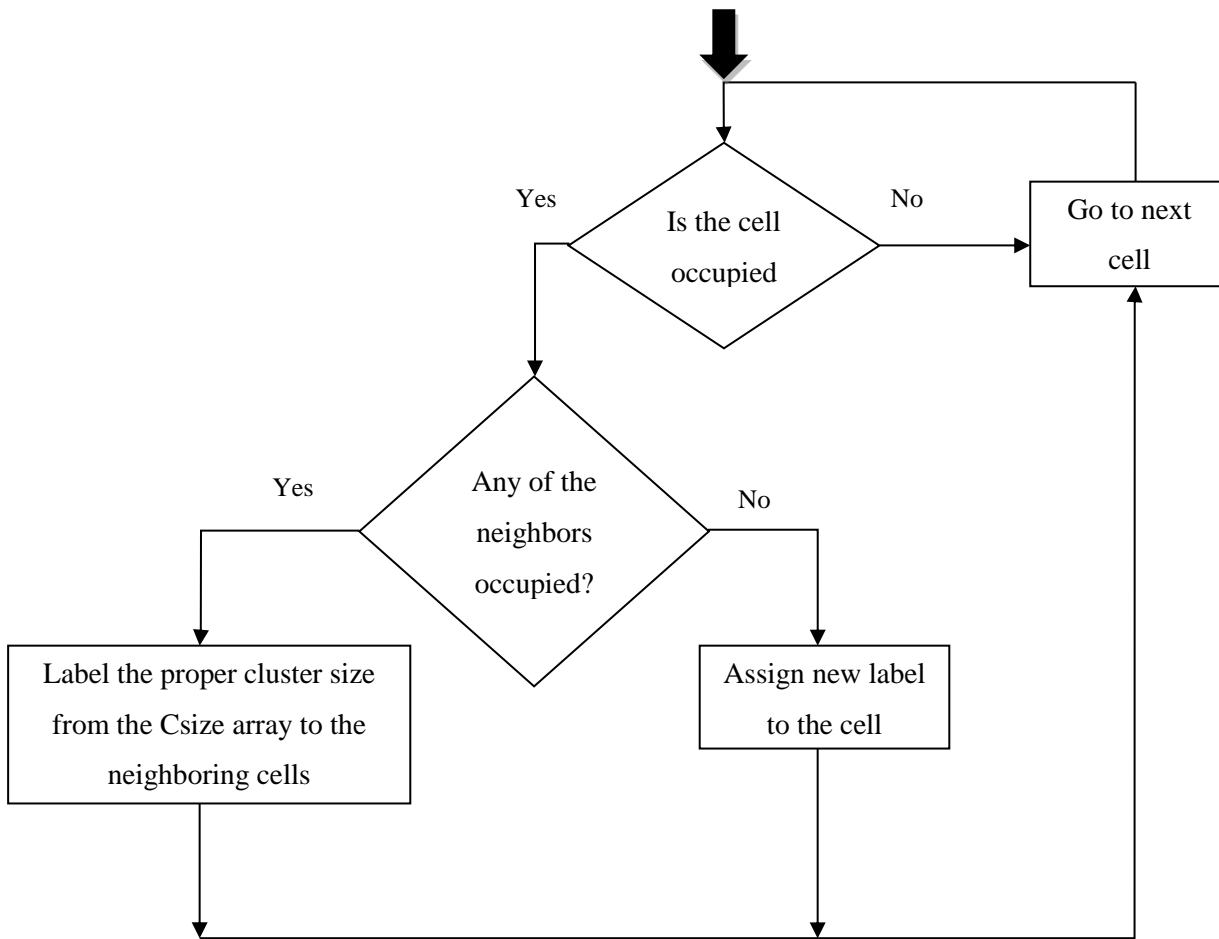


Figure 3-7: Flow chart of classical HK algorithm

Csize Array Procedure:

Csize contains two types of values:

- Positive value: number of members associated with this cluster label.
- Negative value: label redirection. All of the clusters with negative value belong to the other clusters.

Figure 3-8 explains the purpose and function of the Csize array for 2-D clustering. As shown in Figure 3-8(a), cluster 1 has 6 members. Figure 3-8(b-d) has the same pattern to fill the cluster number. Cluster 4 has the same value as 2 in Figure 3-8(e). The same procedure is followed for other clusters. After all the occupied cells are labeled, the Csize array will be scanned again to fix any negative values. In Figure 3-8 (h) the Csize values associated with cluster labels 4 and 5 are -2. This indicates that all cells given the label 4 (and 5) belong to cluster number 2. All cells with the value of 7 belong to cell number 6. The final clustered matrix is demonstrated in Figure 3-8(i).

Matrix

1	1	1	1	0	0	0	0
0	1	1	0	1	0	1	1
0	0	0	1	1	1	0	1
0	0	0	1	1	1	0	0
1	1	1	1	1	0	0	0
0	1	1	0	0	0	1	0
0	0	1	0	0	1	1	1
1	1	0	0	0	1	1	0

Csize

1	6
2	0
3	0
4	0
5	0
6	0
7	0

(a)

Matrix

1	1	1	1	0	0	0	0
0	1	1	0	2	0	3	3
0	0	0	1	1	1	0	1
0	0	0	1	1	1	0	0
1	1	1	1	1	0	0	0
0	1	1	0	0	0	1	0
0	0	1	0	0	1	1	1
1	1	0	0	0	1	1	0

Csize

1	6
2	1
3	2
4	0
5	0
6	0
7	0

(b)

Matrix

1	1	1	1	0	0	0	0
0	1	1	0	2	0	3	3
0	0	0	1	1	1	0	1
0	0	0	1	1	1	0	0
1	1	1	1	1	0	0	0
0	1	1	0	0	0	1	0
0	0	1	0	0	1	1	1
1	1	0	0	0	1	1	0

Csize

1	6
2	1
3	2
4	0
5	0
6	0
7	0

(c)

Matrix								Csize	
1	1	1	1	0	0	0	0	1	6
0	1	1	0	2	0	3	3	2	1
0	0	0	4	1	1	0	1	3	2
0	0	0	1	1	1	0	0	4	1
1	1	1	1	1	0	0	0	5	0
0	1	1	0	0	0	1	0	6	0
0	0	1	0	0	1	1	1	7	0
1	1	0	0	0	1	1	0		

(d)

Matrix								Csize	
1	1	1	1	0	0	0	0	1	6
0	1	1	0	2	0	3	3	2	3
0	0	0	4	2	1	0	1	3	2
0	0	0	1	1	1	0	0	4	-2
1	1	1	1	1	0	0	0	5	0
0	1	1	0	0	0	1	0	6	0
0	0	1	0	0	1	1	1	7	0
1	1	0	0	0	1	1	0		

(e)

Matrix								Csize	
1	1	1	1	0	0	0	0	1	6
0	1	1	0	2	0	3	3	2	7
0	0	0	4	2	2	0	3	3	3
0	0	0	2	2	2	0	0	4	-2
1	1	1	1	1	0	0	0	5	0
0	1	1	0	0	0	1	0	6	0
0	0	1	0	0	1	1	1	7	0
1	1	0	0	0	1	1	0	8	

(f)

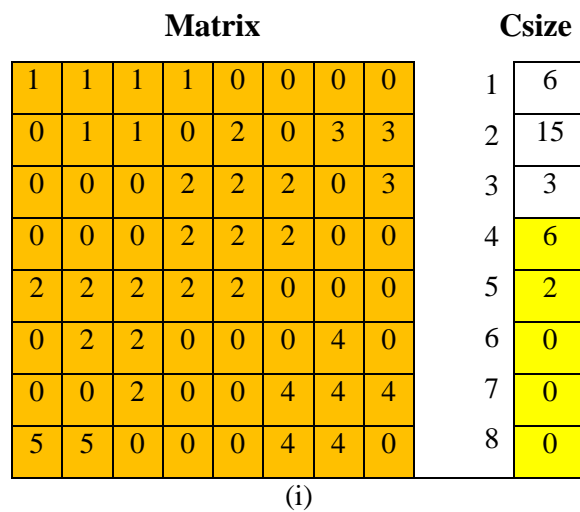
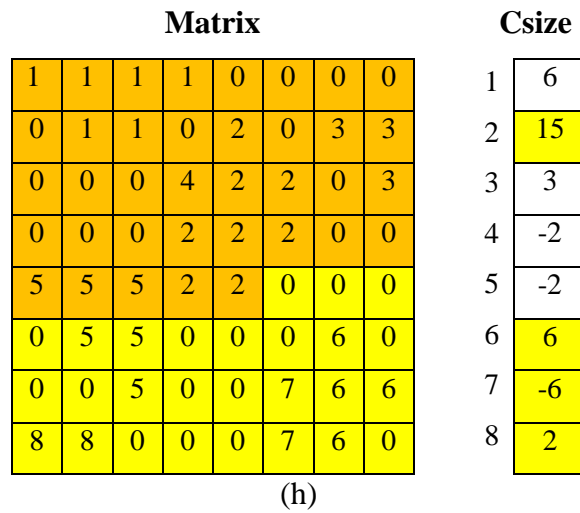
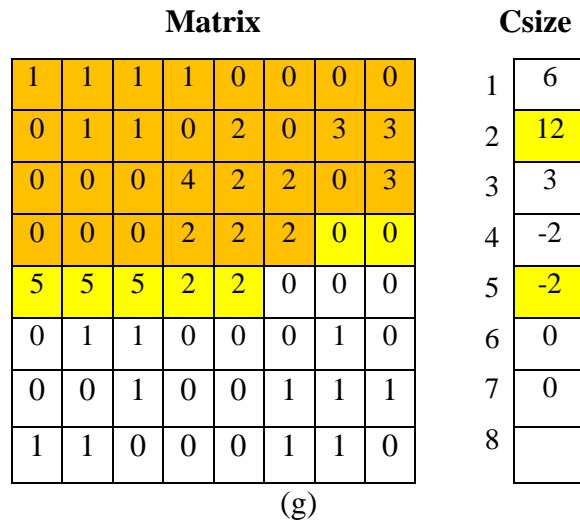


Figure 3-8: Csize procedure in HK algorithm

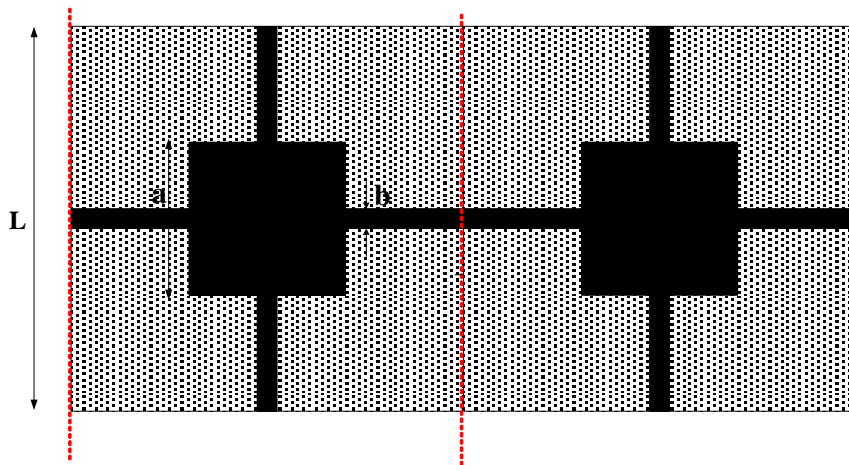
In D-PNM, Cells may be invaded by a non-wetting phase via matrix or secondary pores as explained in section 3.2. Attention must be given to the fact that a cell may be found “open” as a result of containing a vug that can be invaded by the non-wetting phase at a given stage in the invasion process, but is not connected to the secondary porosity of one or more of its neighboring cells. This necessitates additional conditions to be placed on the classical HK technique. These conditions consider the connectivity between the neighbors. After this connectivity between neighbors is obtained, the connected neighbors are marked with the value one in the matrix and other cells are labeled as zero.

Consider two neighboring cells with connected vugs (examined by checking the probability of finding the connection between two cells section 3.1.3). In this situation, if the input capillary pressure (OpenPres) is greater than breakthrough capillary pressure of the vug (Pcbtvug), the two cells are connected through the vugs as illustrated in Figure 3-9 (a). However, in the circumstances of disconnected vugs, if the capillary pressure is greater than break through capillary pressure of the matrix (Pcbtmat), the vugs will be connected through the matrix as represented in Figure 3-9(b). For this reason, three different situations govern the modeling of the open cells:

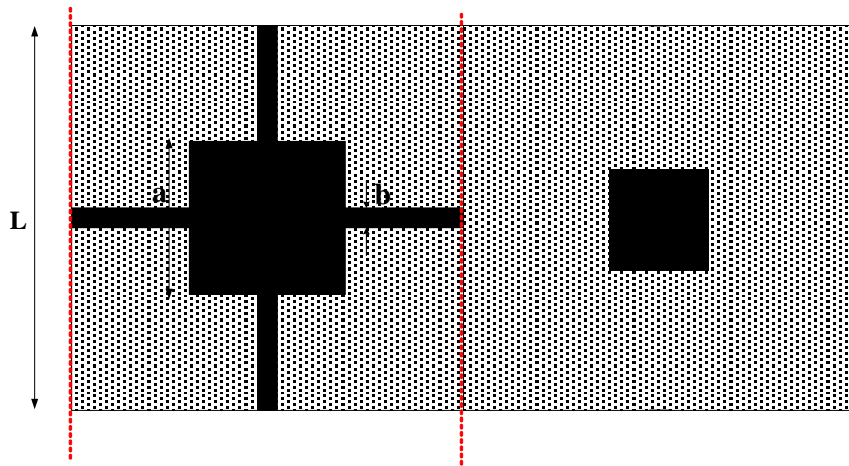
- If (OpenPres>Pcbtvug and OpenPres<Pcbtmat)
- Cell value=1
- Else if OpenPres>Pcbtmat
- Cell value=2
- Else
- Cell value=0
- End

Then there is a matrix with 3 values which is desired to be clustered. In this step, 3x3x3 cells are considered. The cells could be written as 3x3x3 matrixes:

$$\textcircled{2} \quad \begin{bmatrix} 1 & 0 & 1 \\ 2 & 1 & 0 \\ 0 & 2 & 0 \end{bmatrix} \begin{bmatrix} 0 & 1 & 1 \\ 0 & 0 & 0 \\ 0 & 2 & 0 \end{bmatrix} \begin{bmatrix} 0 & 0 & 1 \\ 0 & 0 & 0 \\ 0 & 1 & 2 \end{bmatrix}$$



(a)



(b)

Figure 3-9: Connectivity between neighboring cells

Each cell has three neighbors located on the left, under and inside, in three different dimensions as displayed in Figure 3-10. Two neighboring cells may be open or not open (indicated as one or zero). They also may be connected or disconnected (one or zero). The model will assign two neighbors in the same cluster only if the multiplication of these two conditions, open and connected, equals one. Similar procedure to the classical HK for checking the matrix and Csize would be used after this point.

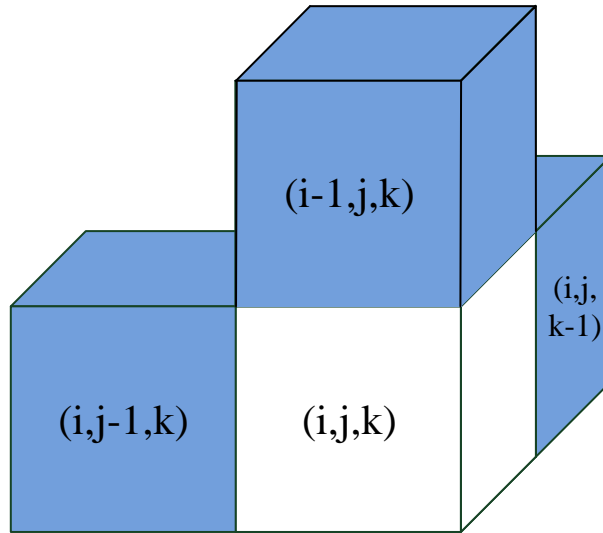


Figure 3-10: nearest three neighbors

3.2.1.3 Accessible Clusters

After determining the open clusters, cells belonging to the clusters that are linked to the inlet face of the network are considered as accessible clusters. To obtain accessible cells, initially, the surface which is employed to drain the wetting phase from the network (either one of x, y or z) is chosen. The code is programmed to distinguish the clusters connected to the inlet face and make the other ones zero. The work flow is represented in Figure 3-11.

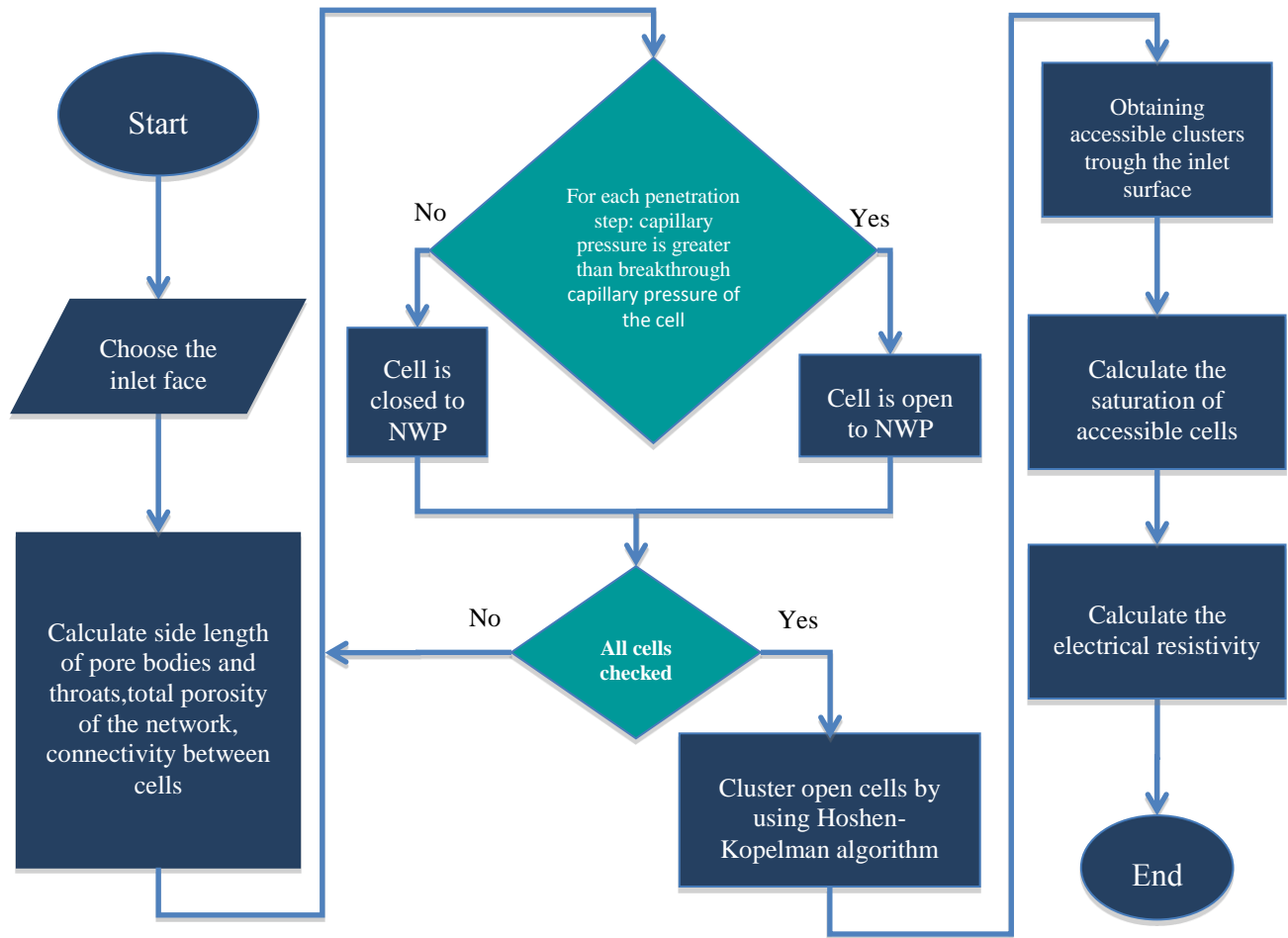


Figure 3-11: Work flow of the model to find the accessible cluster through the inlet surface

3.2.2 Fluid Saturation Calculations

Determination of the water saturation of the D-PNM for each capillary pressure step is explained in this section. This is done in two stages. Initially saturation of each accessible cell's is estimated. Then, the total saturation of the DPNM is computed as the weighted average of individual cell saturation values.

3.2.2.1 Saturation of Each Open Cell

The non-wetting phase saturation in each accessible cell is calculated as the following average [20]:

$$S_{nw} = \frac{\phi_v S_{vnw} + [1 - \phi_v] \phi_m S_{mnw}}{\phi_s} \quad (3-5)$$

where ϕ_v is the vuggy porosity, S_{vnw} is the non-wetting phase saturation in the secondary pore space, ϕ_m is the matrix porosity, S_{mnw} is the non-wetting phase saturation in the matrix, and ϕ_s is the overall cell porosity. ϕ_v is obtained from the inverse Weibull distribution for each cell and ϕ_m is assumed to be uniform for all cells in network as is explained in section 3.1.2. To calculate ϕ_s , the following equation is employed [20]:

$$\phi_v = \frac{\phi_s - \phi_m}{1 - \phi_m} \quad (3-6)$$

The next two sections explain precisely how to obtain S_{vnw} and S_{mnw} .

3.2.2.2 Vug Saturation

Due to the angular cross-sectional shape of the vug bodies and throats in the D-PNM, the wetting phase is not displaced completely by the non-wetting phase upon invasion of the secondary pores. Rather, the corners of vug pore throats and bodies retain some amount of wetting phase when they are first invaded. This so-called ‘‘corner’’ saturation decreases further as the capillary pressure is increased [23].

For each capillary pressure step, the volume at each corner of the pore throats and pore body, that is not filled with the non-wetting phase, is determined using the following approximate equation [27]:

$$V_{co} = \left(\frac{b}{2}\right) R' l_{co} F_2(\theta_R) \quad (3-7)$$

where V_{co} is volume of unfilled corners, l_{co} is the length of the corner, and b is the size length of the throats (it could be the length of the vug body (a) for the vug body volume). $F_2(\theta_R)$ is

obtained from equation (2.7) and R' , the dimensionless radius of curvature of the interface, is determined by the Laplace equation:

$$P'_c = \frac{1}{R'} \quad (3-8)$$

where P'_c is the dimensionless capillary pressure that is calculated for each penetration step by equation (2.9).

The wetting phase volume remaining within the secondary pore space in each cell after this space has been invaded by the non-wetting phase is determined by the following equation:

$$V_{co}^{vug} = V_{co}^{vugbody} + V_{co}^{throats} \quad (3-9)$$

Each cell has one cubic pore body and six pore throats. Each pore body has eight corners and the total volume of unfilled corners for vug body is determined from equation (3-10). Moreover, each throat has four corners (total of twenty four corners in each cell) and $V_{co}^{throats}$ is calculated by equation (3-11), where the function F_2 is defined by equation (2-7).

$$V_{co}^{vugbody} = 8 \left(\left(\frac{a}{2} \right) R' \right)^2 a F_2(\theta_R) \quad (3-10)$$

$$V_{co}^{throats} = 24 \left(\left(\frac{b}{2} \right) R' \right)^2 \left(\frac{1-a}{2} \right) F_2(\theta_R) \quad (3-11)$$

$$V_{co}^{vug} = 24 \left(\left(\frac{b}{2} \right) R' \right)^2 \left(\frac{1-a}{2} \right) F_2(\theta_R) + 8 \left(\left(\frac{a}{2} \right) R' \right)^2 a F_2(\theta_R) \quad (3-12)$$

Therefore, the total volume of the vug (V^{vug}) is equal to:

$$V^{vug} = V^{throats} + V^{vugbody} \quad (3-13)$$

$$V^{vug} = 6b^2 \frac{(l-1)}{2} + a^3 \quad (3-14)$$

The above equations are employed to calculate the vug saturation by:

$$S_{v_{mw}} = \frac{1 - V_{co}(vug)}{V(vug)} \quad (3-15)$$

3.2.2.3 Matrix Saturation

To identify the non-wetting phase saturation of the matrix, the wetting phase saturation is obtained from a Brooks-Corey model of matrix capillary pressure [20]:

$$P_c^* = S_{weff}^{-\alpha} \quad (3-16)$$

where S_{weff} is effective wetting phase saturation of matrix. P_c^* is the reduced capillary pressure and is calculated from:

$$P_c^* = \frac{P_c}{P_c^\circ} \quad (3-17)$$

where P_c° is the breakthrough capillary pressure of the matrix.

The parameter α in equation (3-16) may be estimated from experimental mercury porosimetry data and S_{weff} is obtained by:

$$S_{weff} = P_c^{*-\alpha} \quad (3-18)$$

$$S_{weff} = \frac{S_w - S_{wr}}{1 - S_{wr}} \quad (3-19)$$

where S_w is the wetting phase saturation of the matrix and S_{wr} is a residual wetting phase saturation. Both α and S_{wr} are treated as adjustable parameters in the D-PNM. By substituting the input capillary pressure and breakthrough capillary pressure in equation (3-17), P_c^* is determined. By substituting achieved P_c^* value in equation (3-18) S_{weff} is obtained. Adopting the estimated S_{weff} and S_w is computed with equation (3-19).

3.2.2.4 Total Saturation for Accessible Cells

The non-wetting phase saturation of the DPNM for each capillary pressure step is obtained as the following weighted average equation:

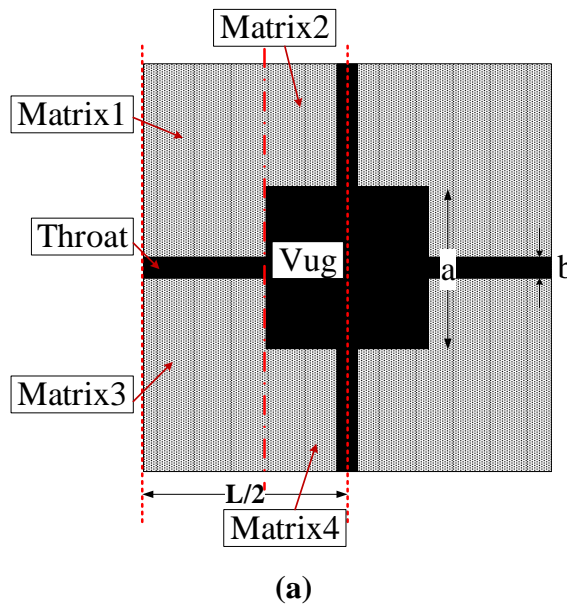
$$S_{nw} = \frac{\sum_{all\ cells} S_{nw}(x, y, z) \phi(x, y, z)}{\sum_{all\ cells} \phi(x, y, z)} \quad (3-20)$$

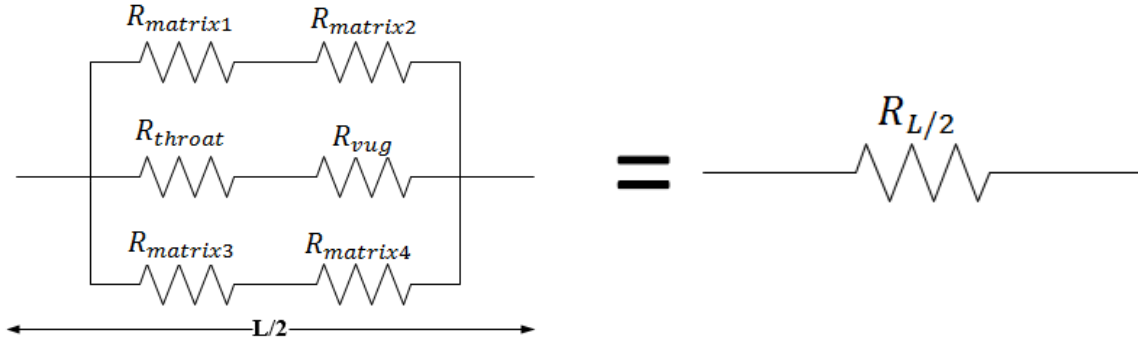
In D-PNM only the accessible cells are non-zero, therefore the saturation of accessible cells is multiplied by their porosity and added together. The value is then divided by total porosity of the model to obtain the total saturation for the network.

3.3 Computation of Resistivity Index

3.3.1 Resistivity of a Single Cell

The electrical resistivity of each cell is isotropic and is determined by the assumption that conduction through matrix is in parallel with conduction through secondary pores, as explained in equation (3-21), equation (3-22) and Figure 3-12(a - b) presented below.





(b)

Figure 3-12: (a) Half-cell resistivity along one direction considering; (b) conduction through matrix in parallel with conduction through secondary pores.

$$R_{L/2} = R_{matrix} || (R_{throat} + R_{vug}) \quad (3-21)$$

$$\frac{1}{R_{L/2}} = \frac{1}{R_{matrix}} + \frac{1}{(R_{throat} + R_{vug})} \quad (3-22)$$

All of R_{matrix} , R_{throat} and R_{vug} are functions of water saturation. To determine R_{matrix} Archie's law, with identified m and n (described in section 1.1.1), is implemented.

$$R_t = R_w \phi^{-m} S^{-n}$$

where R_t is the saturated matrix resistivity, R_w resistivity of a volume of brine of identical dimensions, ϕ is porosity of the rock and S is the rock saturation. $R_{matrix1}$ and $R_{matrix2}$ are equal to $R_{matrix3}$ and $R_{matrix4}$ respectively.

The half-cell resistances R_{throat} and R_{vug} are computed by

$$R = \rho \frac{l}{A} \quad (3-23)$$

where ρ is the electrical resistivity, l is the length of the conductor and A is the cross sectional area of the conductor. Similarly for R_{throat} and R_{vug} half-cell) we have:

$$R_{throat} = \rho \frac{L - a}{2 A_{throat}} \quad (3-24)$$

$$R_{vug} = \rho \frac{a}{2 A_{vug}} \quad (3-25)$$

where A_{throat} and A_{vug} are cross-sectional areas occupied by the conducting aqueous phase. Prior to drainage of the wetting phase from the secondary pore space in a cell, the value of R_{throat} and R_{vug} are calculated from the following equations:

$$R_{throat} = \rho \frac{L - a}{2 b^2} \quad (3-26)$$

$$R_{vug} = \rho \frac{a}{2 a^2} \quad (3-27)$$

As the wetting phase is further drained from the vugs with increasing capillary pressure, the cross sectional areas A_{throat} and A_{vug} decrease according to the equations (3-28) and (3-29). The computation of these areas for each capillary pressure is based on the radius of curvature of the interfaces residing in the corners, which change with capillary pressure according to equation (3-8). Equations (3-28) and (3-29) explain the effect of radius change on the cross sectional area of the vug bodies and throats.

$$A_{throat} = 2bR^2F_2 \quad (3-28)$$

$$A_{vug} = 2aR^2F_2 \quad (3-29)$$

The resistivity of each cell within the D-PNM is modeled by two half-cells in orthogonal directions. It is assumed that three orthogonal plates will divide one cell, which results in six resistors as represented in Figure 3-13[28].

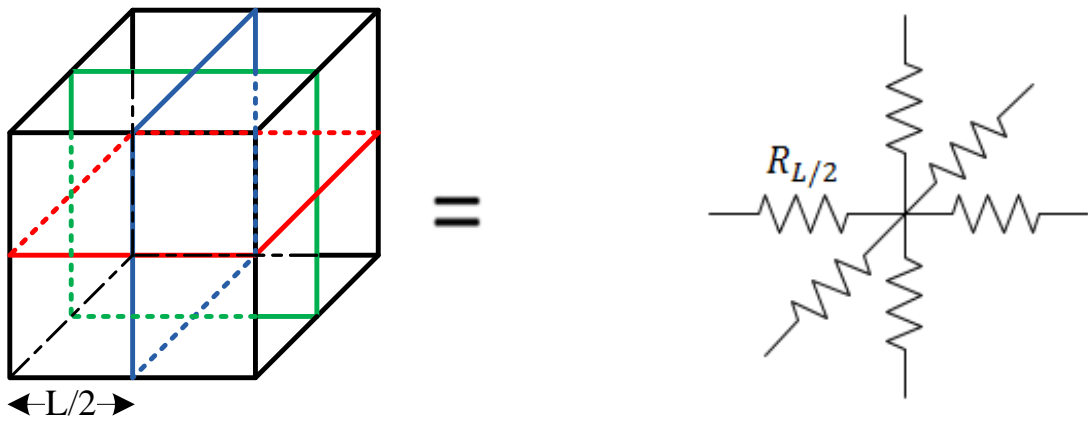
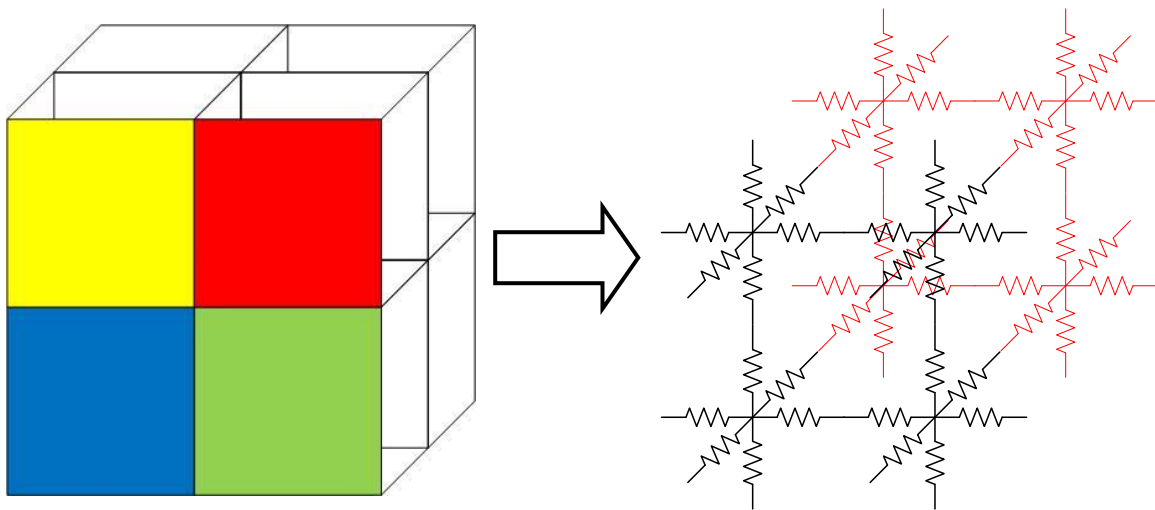
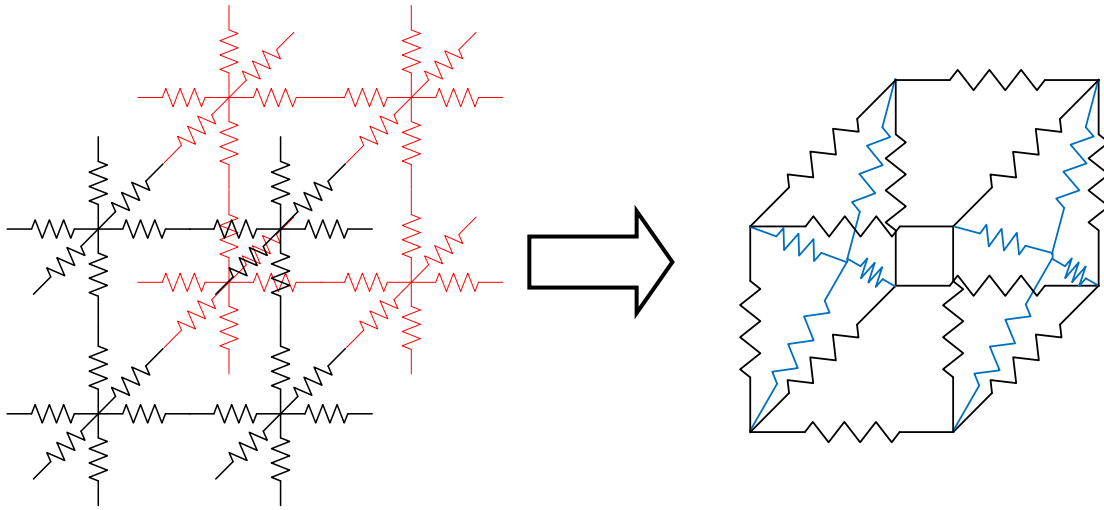


Figure 3-13: Single cell represented in 3D by six identical resistors.

The electrical resistivity of the entire D-PNM is determined by a renormalization approach [29]. Initially eight cells neighboring each other as demonstrated in Figure 3-14(a) are assumed. All of the resistors in eight cells are considered to be in one electrical circuit. Figure 3-15(b) displays electrical schematic of the circuit. Assuming a potential difference of one volt between the beginning and the end point of this circuit, the equivalent resistivity is calculated by Kirchoff's equations for the circuit.



(a)



(b)

Figure 3-14: Calculation of equivalent resistivity of eight neighboring cells

Same approach is employed for the total network as illustrated in Figure 3-15. First, the total network is divided into the groups of eight cells ($2 \times 2 \times 2$), and then the equivalent resistor is calculated for each group of $2 \times 2 \times 2$ cells implementing the above mentioned approach. In this process, by replacing eight resistors with 1 equivalent resistor, the number of cells is decreased into $1/8$ of previous amount. This procedure will be continued until reducing the number of resistors into one resistor which is the equivalent resistivity of the total network (R_t).

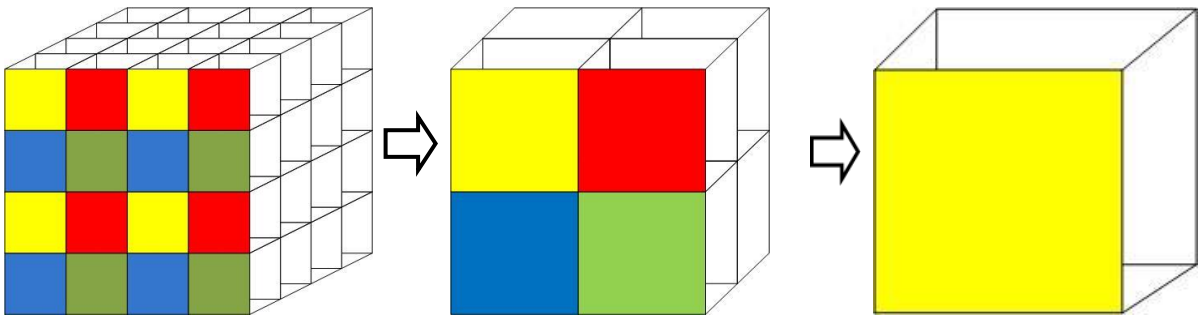


Figure 3-15: Schematic of renormalizing $4 \times 4 \times 4$ cells to one cell

For each penetration step, the resistivity index of the D-PNM (RI) is the specified computed resistivity (R_t) at any saturation over the resistivity of the fully water-saturated rock (R_0) (equation (1-3)). R_0 is the resistivity of the rock at the initial moment (before desaturation state starts).

$$RI = \frac{R_t}{R_0} \quad (1-3)$$

3.4 Computation of Formation Factor

For calculating the formation factor of the D-PNM, Archie's law is employed as described in section 1.1.1.

$$F = \frac{R_0}{R_w} \quad (1-2)$$

where R_0 is the resistivity of the fully water-saturated rock and R_w is the resistivity of the volume of brine of identical dimensions. Calculation of R_0 was explained in the previous section. We compute R_w from (equation (3-23)) by substituting the geometry of the system for length and cross sectional area as follows:

$$R_w = \rho \frac{l(j)}{(l \times i)(l \times k)} \quad (3-30)$$

where j is the number of cells along the direction of transport, i and k are the number of cells in two other directions and l is the side length of each cell.

Chapter 4

Results and Discussion

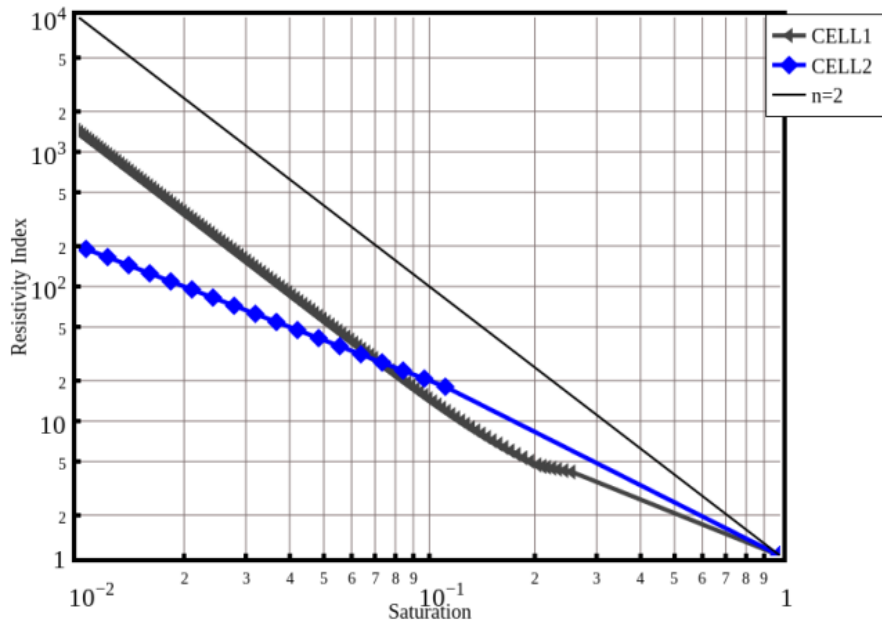
4.1 Model Response

4.1.1 Single Cell Response

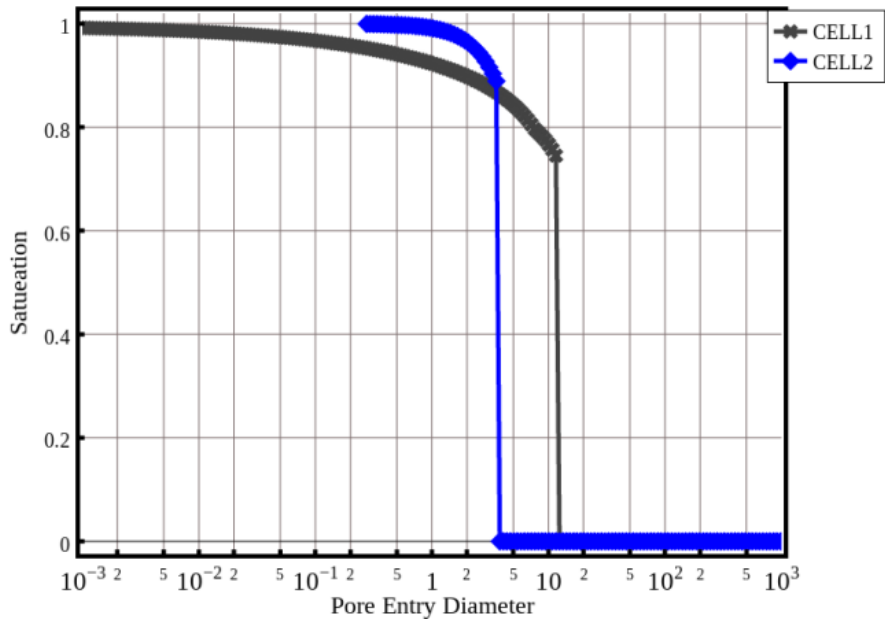
The electrical response of a single cell for two sets of parameters, referred to as CELL1 and CELL2, are presented in Figure 4-1. As it indicated in Table 4-1, both cells contain the same amount porosity, $\phi_s = 0.2$. However, the matrix porosities in the two cells are different; $\phi_m = 0.05$ for CELL1 and $\phi_m = 0$ for CELL2. Furthermore, $R = 0.1$ for CELL1 and $R = 0.03$ for CELL2. The secondary porosity in CELL1 is invaded when S_w is between 0.2 and 0.3. The small plateau until $S_w = 0.2$ is the effect of remaining water in the corners of the vug. At water saturation of about 0.2 the primary porosity (matrix porosity) is invaded and RI exhibits a slope of -2, as expected since Archie behavior with $n = 2$ is assumed for the matrix. The secondary pore space in CELL2 (with no matrix porosity) is invaded at a higher capillary pressure as expected given the smaller value of R , corresponding to $S_w \sim 0.1$. Remaining water in the corners of the secondary pore space is the reason of bending down in the CELL2 resistivity curve. Remarkably, non-Archie behavior is already exhibited by a single cell in the D-PNM, attesting to the importance of accounting for porosity at two different scales.

Table 4-1: Single cell parameters

	$\phi_{total}(\%)$	$\phi_{matrix}(\%)$	R
CELL1	20	0.05	0.1
CELL2	20	0	0.03



(a)



(b)

Figure 4-1: Single cell model response: (a) resistivity index vs. saturation, (b) pore entry diameter distribution

4.1.2 Total Network Model Response

The total network response of the model may be examined in the context of three main model classes; (1) D-PNM with percolating matrix and percolating vugs (PM-PV), (2) D-PNM with percolating matrix and non-percolating vugs (PM-NPV), and (3) D-PNM with non-percolating matrix and percolating vug (NPM-PV). In each of these classes we may further distinguish three different situations based on the relative amount of matrix and secondary porosity; (1) secondary porosity is dominant ($\phi_v \gg \phi_m$) (2) secondary porosity is comparable to matrix porosity ($\phi_v \sim \phi_m$) (3) matrix porosity is dominant ($\phi_v \ll \phi_m$). Figure 4-2 is cartoon representation of one (out of nine) different types of D-PNM realizations, drawn for simplicity as models with 10x10 cells. Secondary porosity, matrix porosity and solid are identified in the following figure. Unlike the cartoons, the results discussed below have been carried out with D-PNM of 32x32x32 cells.

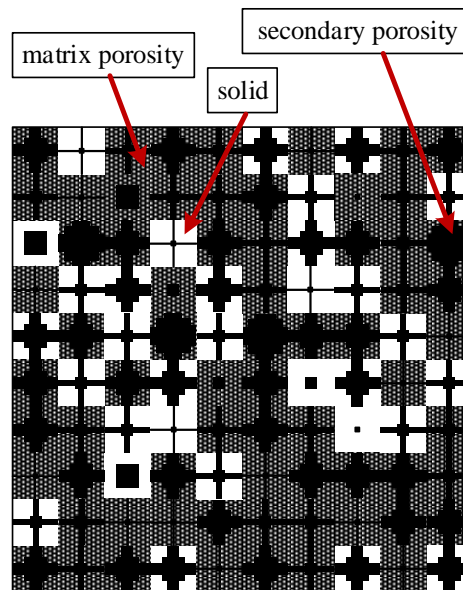


Figure 4-2: DPNM with 10x10 cells

Figure 4-3 shows the behavior of the model with only matrix porosity in case of no secondary porosity. Matrix properties are assumed to be uniform in the simulations presented in this thesis.

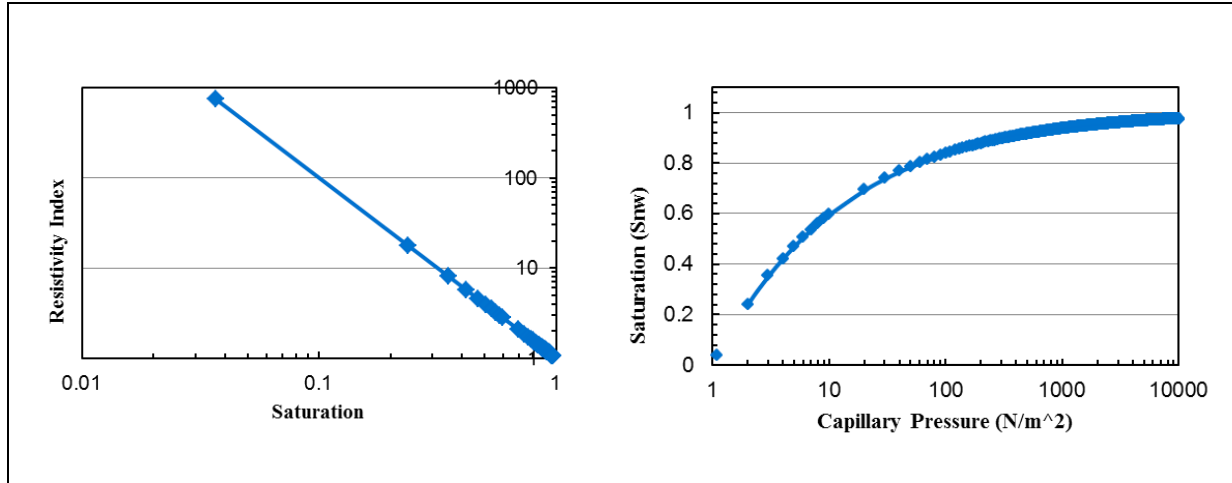


Figure 4-3: Electrical resistivity and capillary pressure properties of the matrix.

4.1.2.1 Percolating Matrix and Percolating Vugs

Figure 4-4 (a), (b) and (c) represent the first class (PM-PV). The responses of the DPNM for this type of pore structure are illustrated in Figure 4-5. The model parameters for these results can be seen in Table 4-2. Figure 4-5(a) shows the response of the first D-PNM member in this class, in which the secondary porosity is significantly higher than the matrix porosity ($\frac{\phi_m}{\phi_v} \sim 0.07$), for two different values of R. In the RI curve, more than ninety percent

of the water is drained from the vugs and almost ten percent from the matrix, because of the significantly higher secondary porosity. Drainage from point (a) to point (b) corresponds with desaturation of the secondary pore space, for which the dependence of resistivity on saturation is weaker than predicted by Archie's law (slope less than -2 on a log-log plot). When most of the vugs have been invaded by the non-wetting phase, at point (c), resistivity increases sharply within a short range of water saturation and until the matrix porosity is first invaded by the non-wetting phase. The sharp increase of resistivity at point (c) is due to the

fact that water in the corners of invaded vugs makes a significant contribution to electrical conductivity – a contribution that depends strongly on water saturation. That is to say, small changes in the total water saturation (due to loss of water from the corners of drained vugs) results in a significant increase of electrical resistivity.

Turning now to the capillary pressure vs. water saturation curve, a smaller value of R shifts the capillary pressure curve to the right. This is expected because for a smaller value of R (recall that $R=b/a$) the throats connecting vugs are smaller and, for this reason, the breakthrough capillary pressure of the vugs is higher. In Figure 4-4(a), the green line representing RI for the D-PNM with smaller R is shifted downward, indicating a weakening of the dependence of resistivity on water saturation. This makes sense because the vug throats are current-carrying paths. Drainage of water from the secondary pore space corresponds to loss of less significant conductors in the D-PNM with lower R . Similarly, the effect of loss of water from the corners of drained vugs is diminished in the D-PNM with lower R .

Figure 4-5(b) shows the response of the second D-PNM member in this class, in which the secondary porosity is comparable to the matrix porosity ($\frac{\phi_m}{\phi_v} \sim 1$), for the same two values of R . About sixty percent of the water is drained from the vugs and forty percent is drained from the matrix. The behavior of the RI curve observed in Figure 4-5(a) is barely evident here because the significant amount of matrix porosity results in significant conduction through the matrix over a broad range of water saturation. A decrease in the value of R causes a “break” in the RI curve and a reduction of the sensitivity of resistivity on saturation. Again, this is understood because drainage of water from the secondary pores is results in loss of less significant conductors (smaller throats). At point (d), the slope is increasing for both values of R when the water saturation is low enough for conduction through water in the corners of drained vugs to compete with conduction through drained matrix.

In the third situation where the matrix porosity is dominant, almost all water is drained from matrix porosity. Changing the value of R does not influence the capillary pressure-

saturation curve and has only a minor impact on the RI. Here, following drainage of ninety percent of the water (point (e)), a bending down is observed in the curves for both values of R . This is because of the water in the cells with negligible matrix porosity. For the smaller value of R , as the throats become smaller, this impact is even smaller.

Table 4-2: PM-PV parameters

PM-PV	ϕ_v	ω	$\frac{\phi_m}{\phi_v}$	f_m^0	$l(\text{cm})$
$\phi_m/\phi_v \ll 1$	0.5	0.8	0.07	0.3	1
$\phi_m/\phi_v \sim 1$	0.135	0.8	1	0.3	1
$\phi_m/\phi_v \gg 1$	0.00135	0.8	100	0.3	1

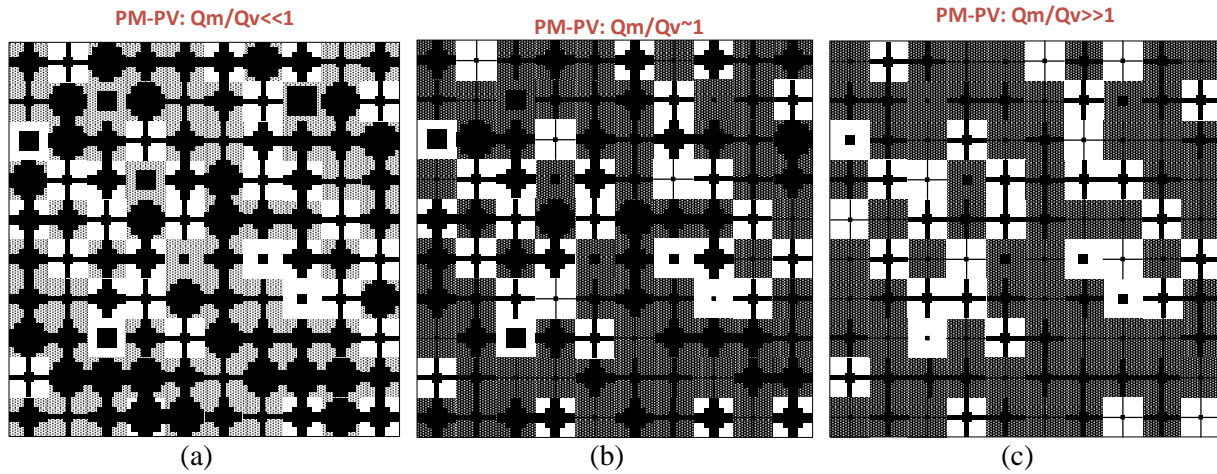
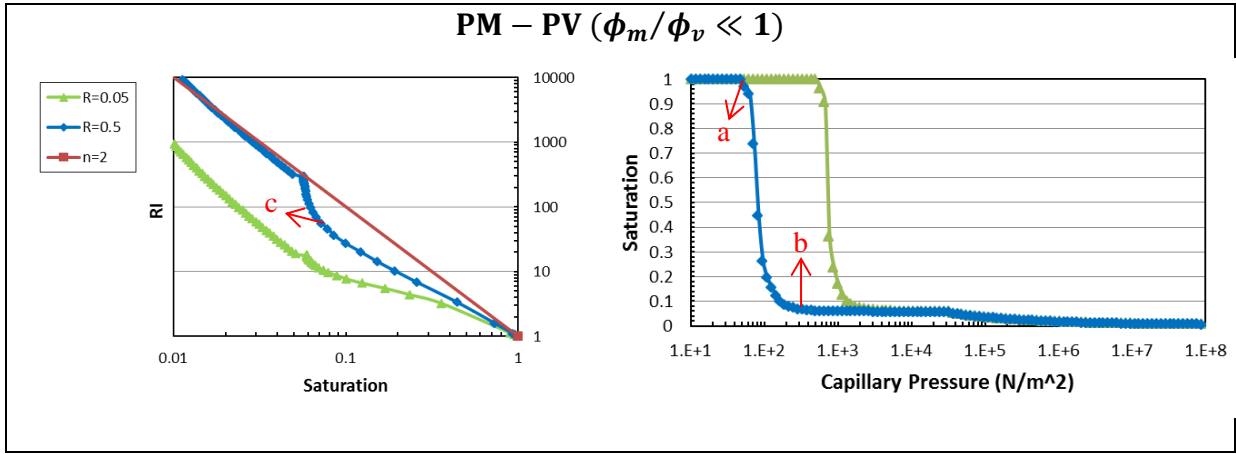
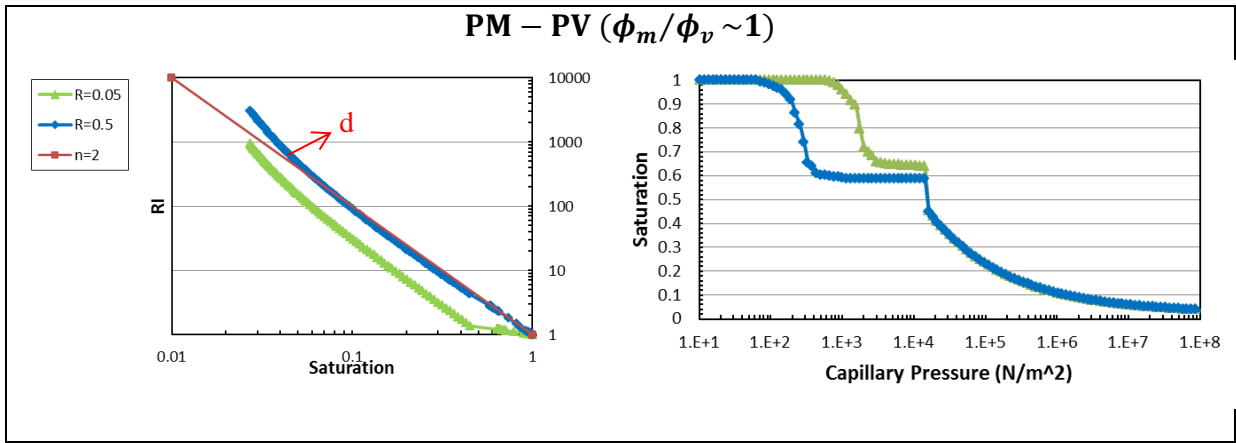


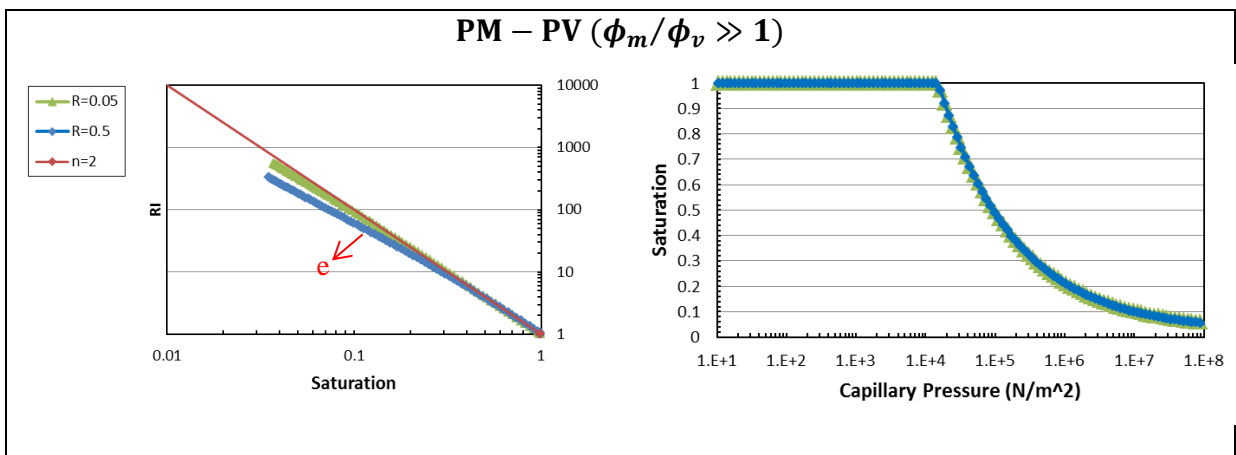
Figure 4-4: DPNM with percolating matrix and percolating vugs.



(a)



(b)



(c)

Figure 4-5: Typical response of the PM-PV class of D-PNM

4.1.2.2 Non-percolating Matrix and Percolating Vugs

Figure 4-6 demonstrates a schematic of DPNM for non-percolating matrix and percolating vugs. In Figure 4-7 the response of the model for the set of parameters listed in Table 4-4 are presented. When the vug porosity dominates over matrix porosity and the matrix is non-percolating, the significance of conduction through the corners of drained vugs is exaggerated, as shown in Figure 4-7 (a). The presence of a significant number of cells with zero matrix porosity means that a significant amount of water can be trapped. The cells with zero matrix porosity are conductive but they are not drained through the vugs. This has the effect of results the slope of the matrix desturation part (above point (f)) greater than -2. The difference between blue and green lines in the RI curve is because of the smaller R (smaller throats) that is mentioned in previous part.

In Figure 4-7 (b-c) the same process occurs, except because of changing the value of ratio ϕ_m/ϕ_v the amount of water in secondary porosity decreases and the amount of water in matrix porosity increases, therefore the matrix starts to invade in lower saturation.

Table 4-3: NPM-PV parameters

NPM-PV	ϕ_v	ω	ϕ_m/ϕ_v	f_m^0	$l(\text{cm})$
$\phi_m/\phi_v \ll 1$	0.5	1	0.01	0.8	1
$\phi_m/\phi_v \sim 1$	0.14	1	1	0.8	1
$\phi_m/\phi_v \gg 1$	0.0014	1	100	0.8	1

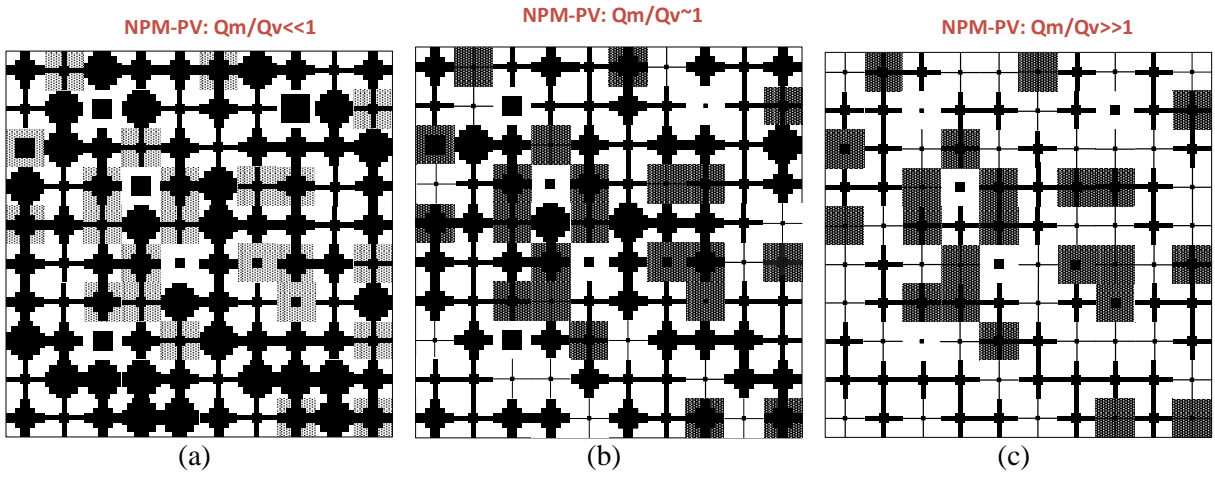
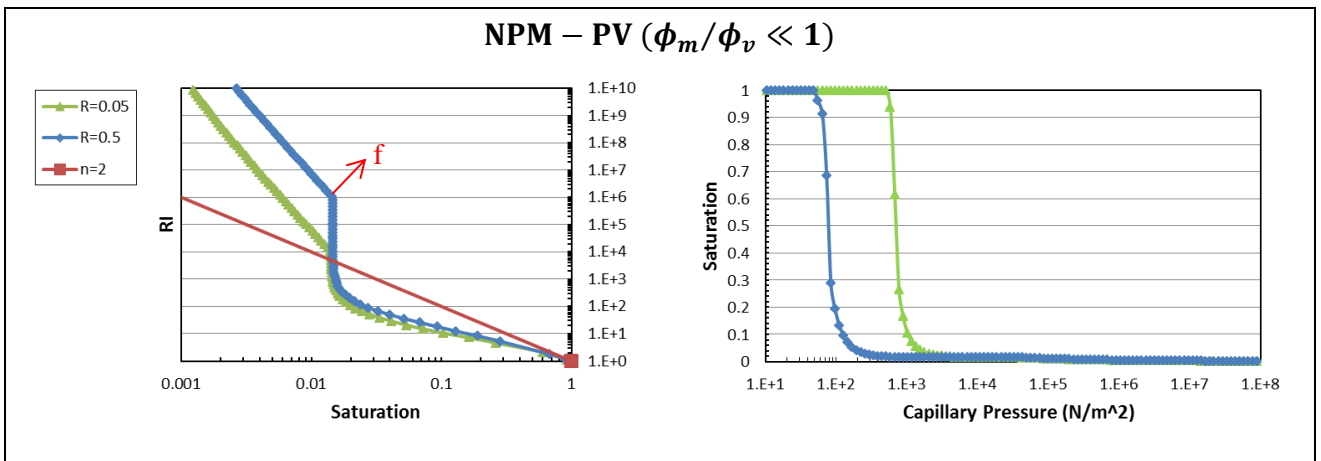
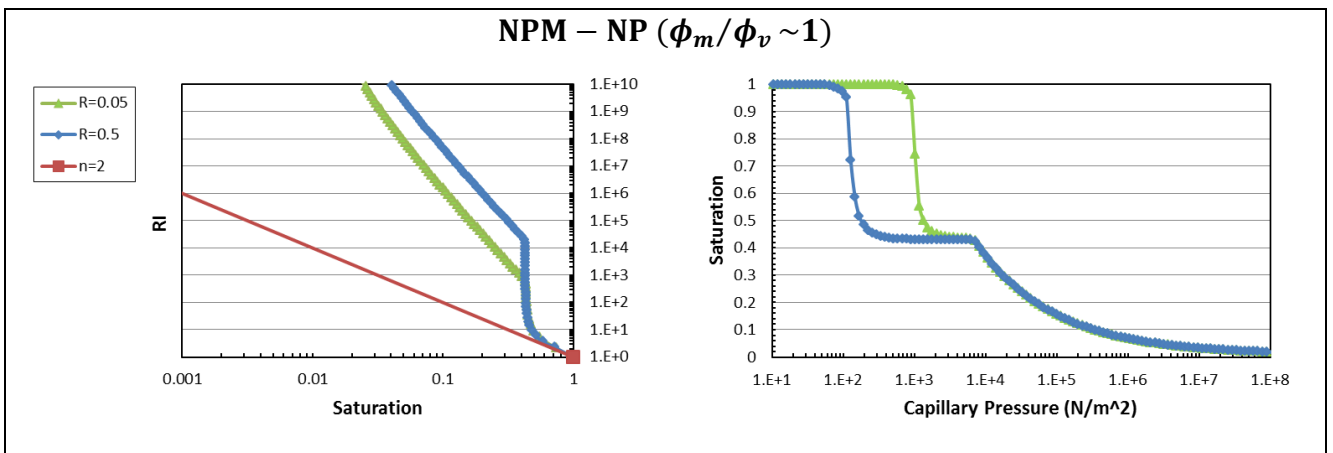


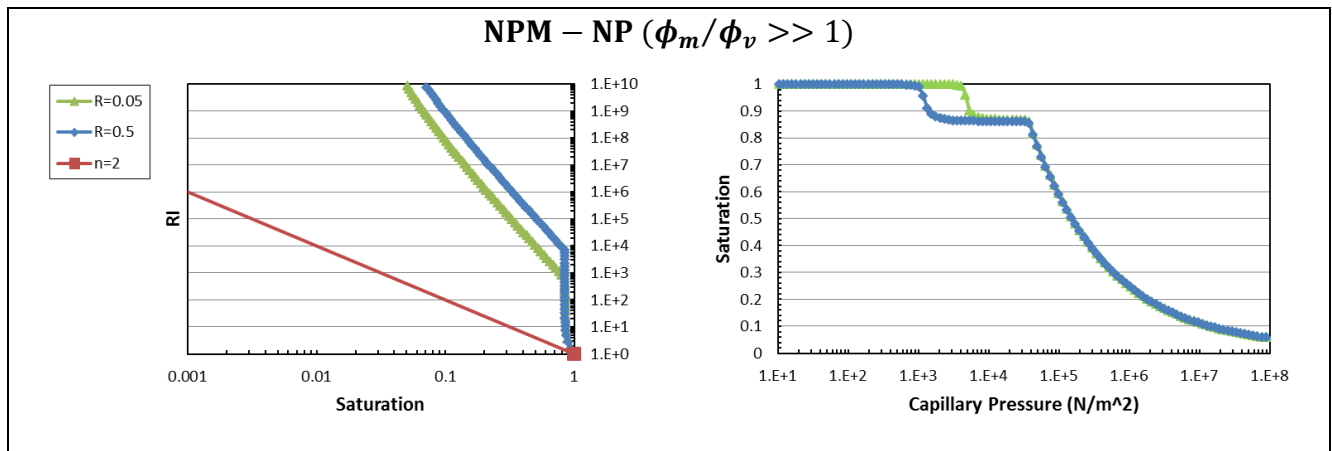
Figure 4-6: DPNM with non-percolating matrix and percolating vugs



(a)



(b)



(c)

Figure 4-7: Typical response of NPM-PV class of D-PNM.

4.1.2.3 Percolating Matrix and Non-percolating Vugs

Figure 4-8 is a schematic of D-PNM with percolating matrix and non-percolating vugs. Typical responses for this class of D-PNM are illustrated in Figure 4-9 for the parameters presented in Table 4-4. A gap between point (g), corresponding to drainage of connected vugs, and point (h), corresponding to the beginning of drainage from the matrix, is evident in Figure 4-8(a). This gap is due to the fact that the vugs are non-percolating. As a result, a significant amount of water held in vugs can be drained only when the matrix is invaded. Because all connected matrix cells are invaded by the non-wetting phase at the same value of capillary pressure, water is lost from the vugs in one step. The sharp rise in resistivity above point (h) is due to the fact that, given the small amount of matrix porosity, water in the corners of drained vugs is the main conductor of electric current. As discussed before, the resistivity of water in the corners depends sensitively on saturation.

As shown in Figure 4-9 (b), a qualitative similar behavior is observed when matrix and secondary porosity are of the same magnitude. However, in Figure 4-9(c) the RI curve is bending down, which is due to water trapped by cells with zero matrix porosity. In this case the effect of corners would be negligible, as a result of small secondary porosity.

Table 4-4: PM-NPV parameters

PM-NPV	ϕ_v	ω	ϕ_m/ϕ_v	f_m^0	$l(\text{cm})$
$\phi_m/\phi_v \ll 1$	0.5	0.5	0.01	0.3	1
$\phi_m/\phi_v \sim 1$	0.135	0.5	1	0.3	1
$\phi_m/\phi_v \gg 1$	0.00135	0.5	100	0.3	1

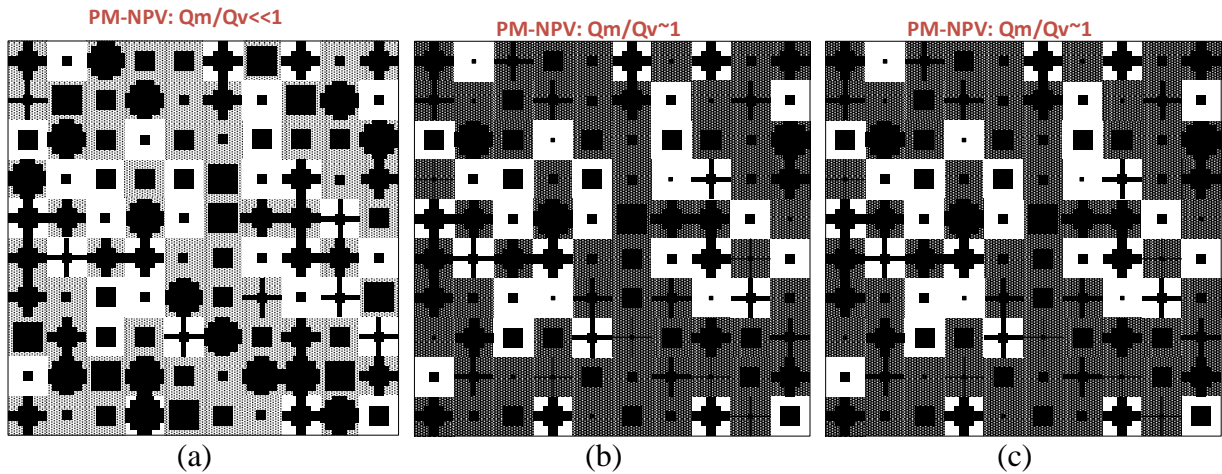
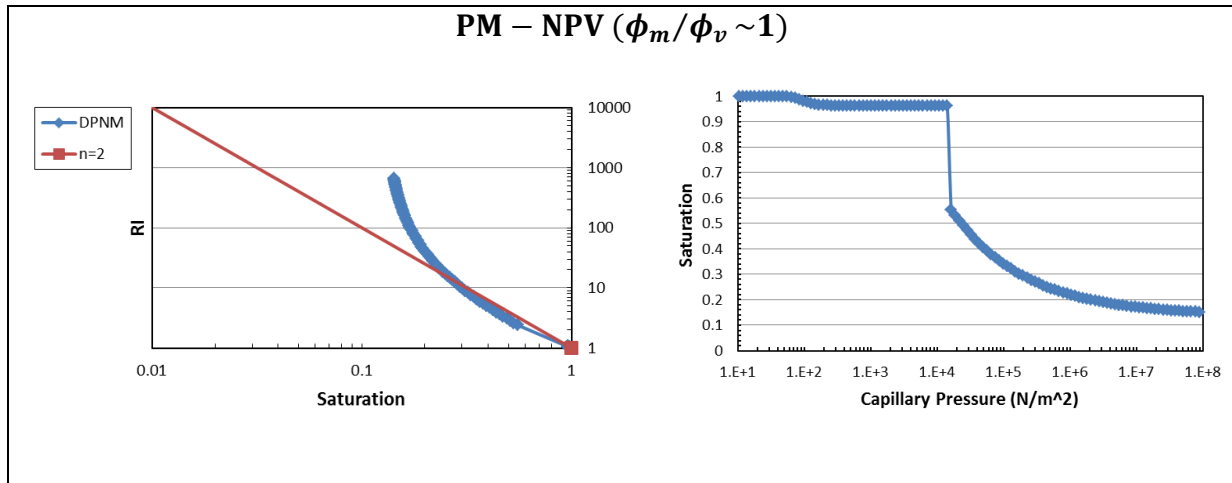


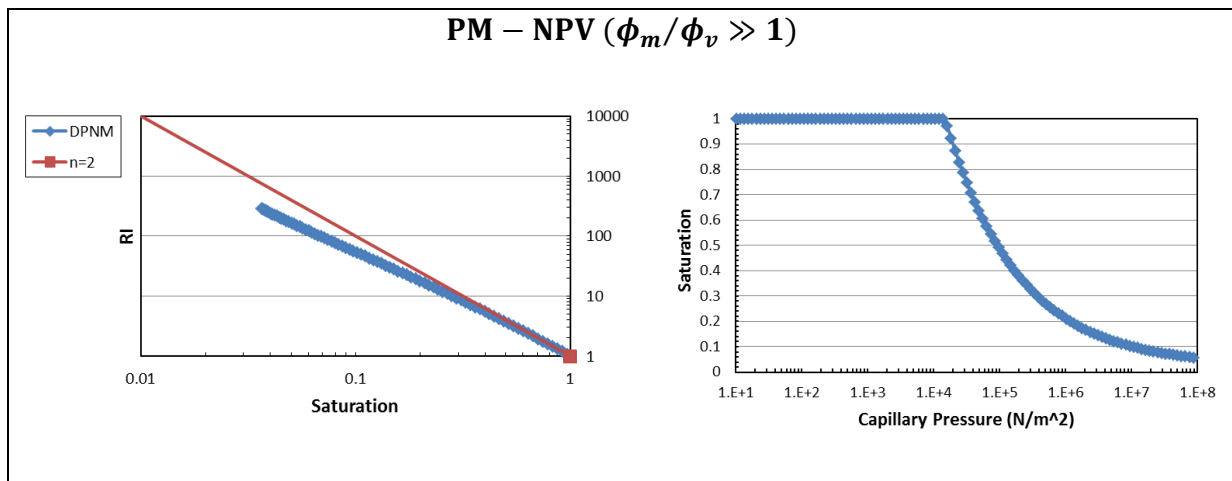
Figure 4-8: DPNM with percolating matrix and non-percolating vugs



(a)



(b)



(c)

Figure 4-9: Model response of PM-NPV type

4.2 Verification of the Model

As indicated in Figure 4-12 and Figure 4-14, the dual pore network describes the electrical resistivity of both Estailades and Lavoux carbonate samples quite well, as is evident from comparison with the experimental data of Bauer et al. (Bauer et al. 2011). The DPNM reproduces the formation factor of both samples (Table 4-5), while being consistent with the pore size distributions determined by mercury porosimetry. Figure 4-11 illustrates the SEM

images of both samples. Table 4-6 represents the DPNM parameters which are employed to obtain the following responses from the model. Note that these fits were obtained by assuming uniform matrix properties and hypothetical vug porosity distributions. The possibility exists to utilize spatially resolved porosity data and will be pursued in future work.

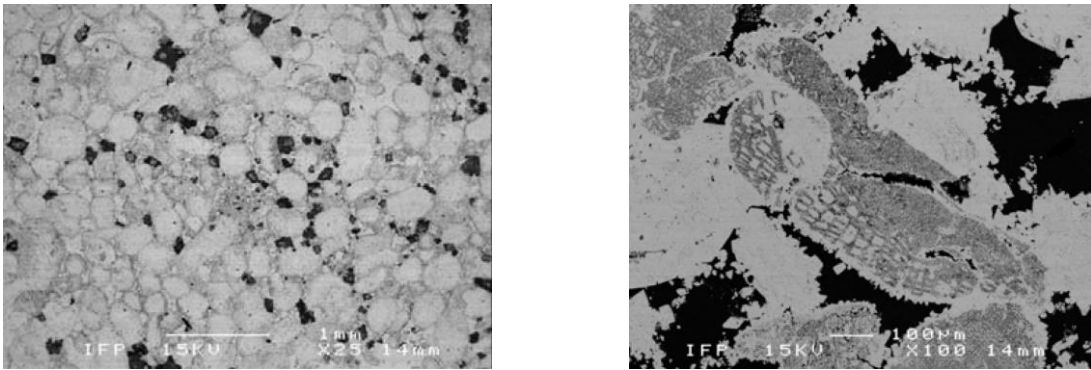


Figure 4-10: The SEM image of Lavoux(left) and Estailade Limestone (right) [17]

Table 4-5: Porosity and formation factor of real samples and DPNM

Sample	$\phi_{total}^{Exp} (\%)$	$\phi_{total}^{DPNM} (\%)$	FF^{Exp}	FF^{DPNM}
Lavoux	28.7	28.5	13	13.7
Estailades	24.7	23.9	24	27.3

Table 4-6: DPNM parameters

Sample	ϕ_{vug} (%)	ϕ_{matrix} (%)	R	ω	f_m^0	l (μm)
Lavoux	12.65	28	0.4	0.8	0.4	200
Estailades	15	30	0.25	0.815	0.7	200

4.2.1 Lavoux Carbonate Sample Verification

Figure 4-12 illustrates the DPNM response for the network of 32x32x32 cells. These results are consistent with the experimental resistivity response of Lavoux sample [17]. The total porosity is 28.5%, 12.65% of secondary pore space and 28% of matrix porosity, both matrix and secondary pore space networks are percolating Figure 4-4 (b). Figure 4-11 shows the vug distribution used in the model. More than sixty percent of the water is drained through the secondary porosity, and then the remaining water (less than forty percent) is drained from the matrix porosity. In experimental pore entry diameter curve the slight variation in the slope occurs at saturation of about fifty percent. In addition, response in DPNM is in saturation of about forty percent. In the context of the D-PNM, in the case of percolating matrix, conduction through the matrix pores causes a leveling off the resistivity index at lower saturations.

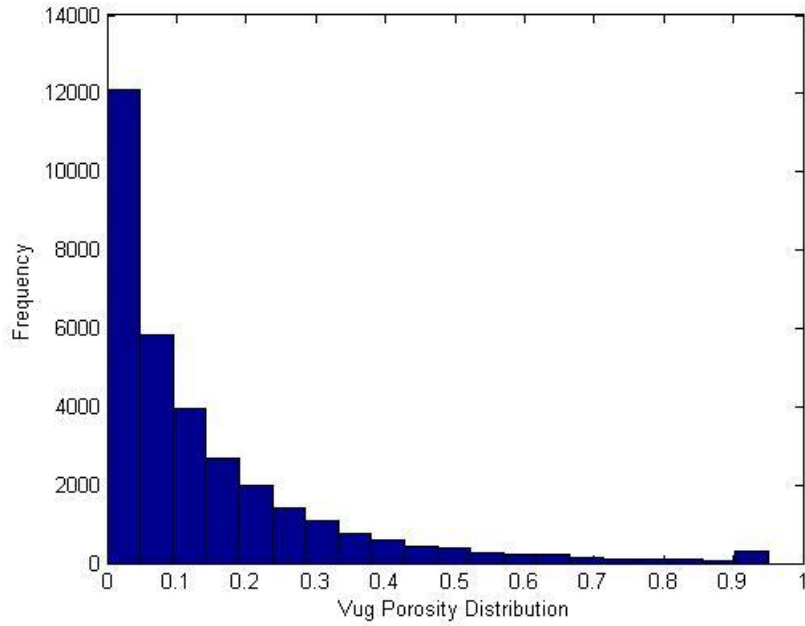
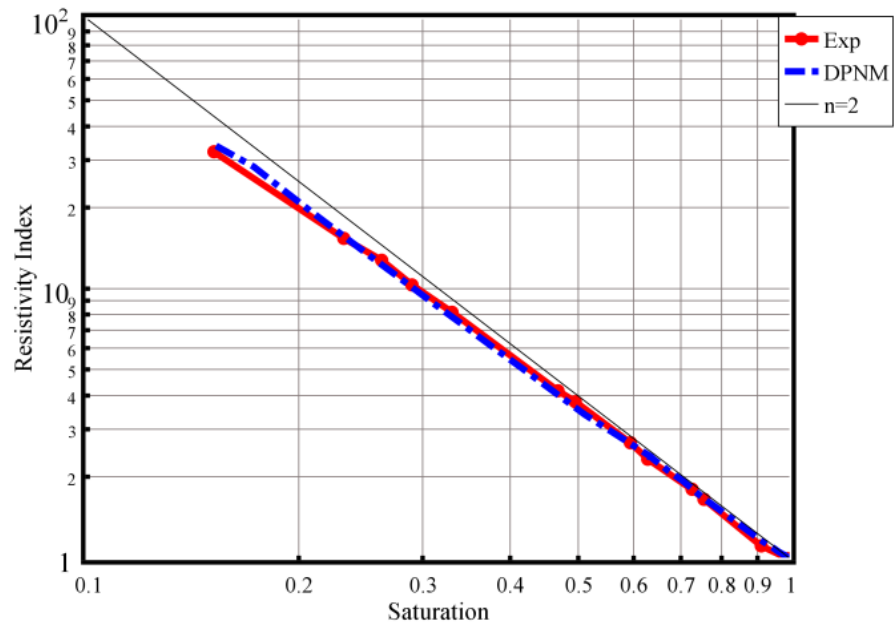
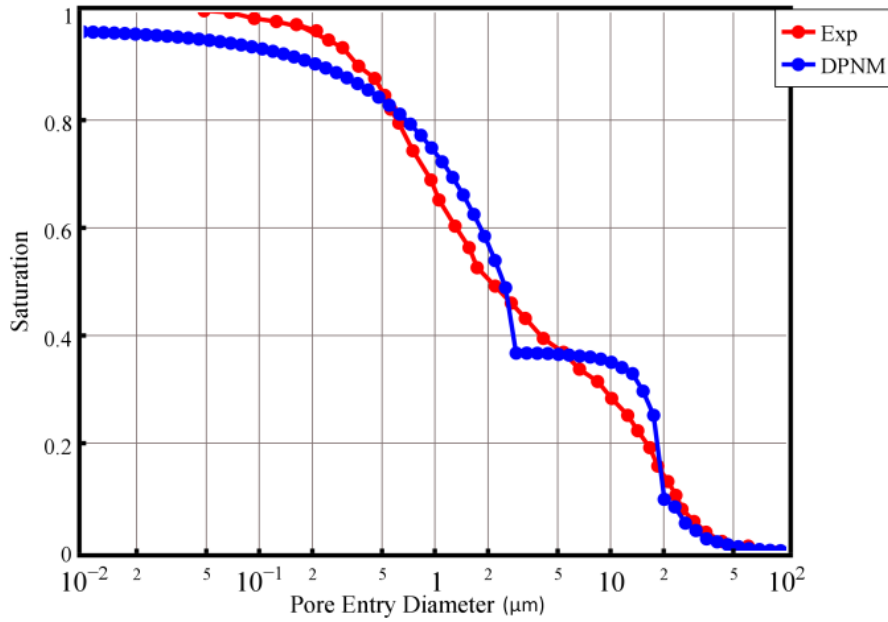


Figure 4-11: Vug distribution for Lavoux sample



(a)



(b)

Figure 4-12: Lavoux carbonate sample: (a) resistivity index vs. saturation, (b) pore entry diameter distribution

4.2.2 Estailades Carbonate Sample

The Estailades sample is represented by a percolating secondary pore space network superimposed on non-percolating matrix Figure 4-14 (b). These results are consistent with the experimental resistivity response of Estailades sample [17]. Figure 4-15 illustrates the vug distribution in this set of parameter. About forty percent of the water is drained through the secondary porosity and more than sixty percent is drained from the matrix porosity. In the context of the D-PNM, the curving upwards of the resistivity index near forty percent water saturation for the Estailades sample occurs because of increasing resistivity of water remaining in drained secondary pore spaces. The above mentioned effect is observable particularly while the matrix porosity is non-percolating.

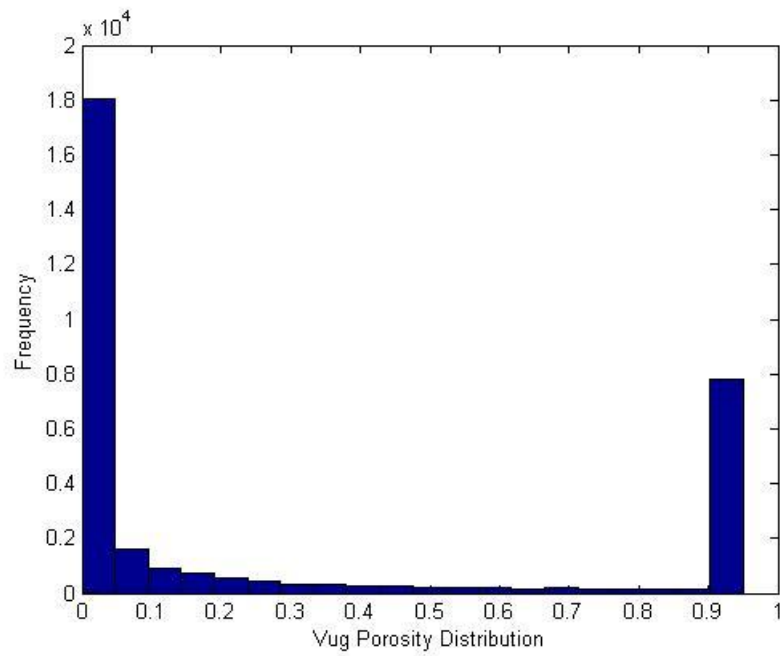
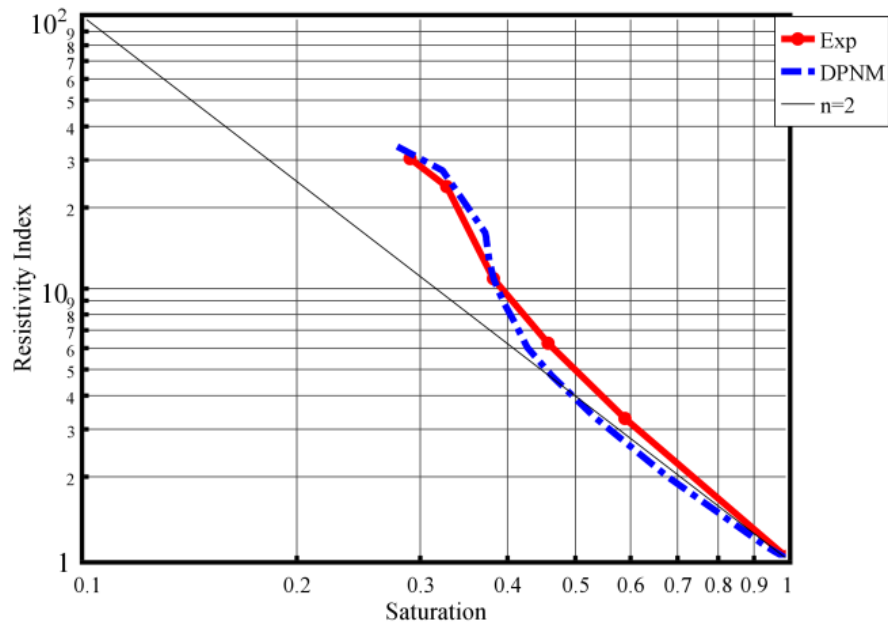
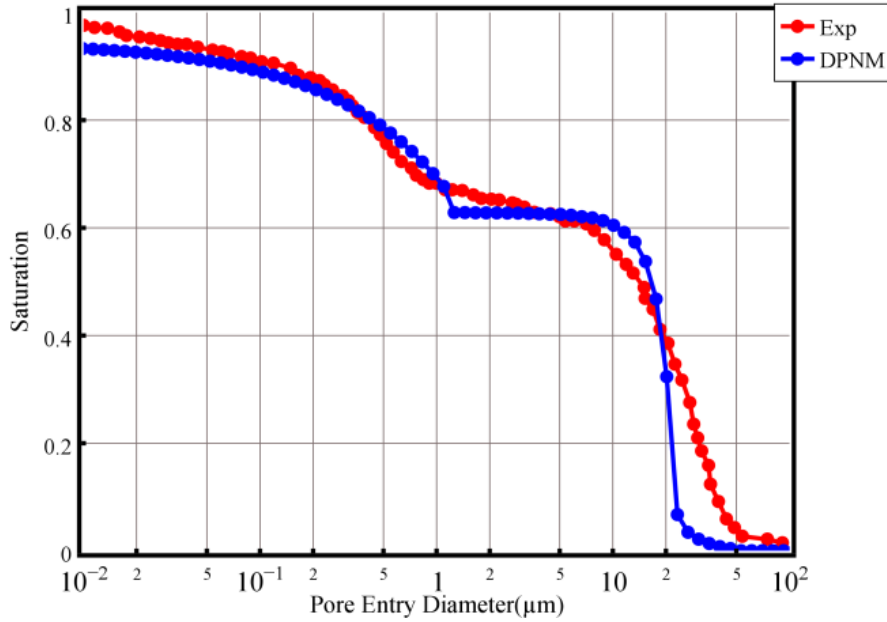


Figure 4-13: Vug distribution for Estailades sample



(a)



(b)

Figure 4-14: Estailades carbonate sample: (a) resistivity index vs. saturation, (b) pore entry diameter distribution.

4.2.3 Parametric Study

Figures 4-15 to 4-18 demonstrate the D-PNM resistivity index variation via saturation change for Estailades carbonate sample considering sensitivity to model parameters. These parameters are including zero matrix porosity fraction, aspect ratio R , and connectivity exponent. These figures indicate remarkable sensitivity of the resistivity index to different D-PNM parameters, demonstrating deviations from Archie's law ($n = 2$).

Figure 4-15 represents the effect of changing the fraction of cells assigned zero matrix porosity (f_m^o), where this fraction is varied from zero to 0.8. As f_m^o increases, the probability increases for water to be trapped within matrix porosity. The results illustrate that for water saturation between ten and sixty percent, the slope may change from less than -2 to higher than -2 by increasing f_m^o . For f_m^o more than 0.7 the matrix is non-percolating. In such instances, as it described in section 4.1.2.2., the continuing drainage of the water remaining

in the corners of vugs causes a sharp increase in electrical resistivity since there is no alternative conduction pathway.

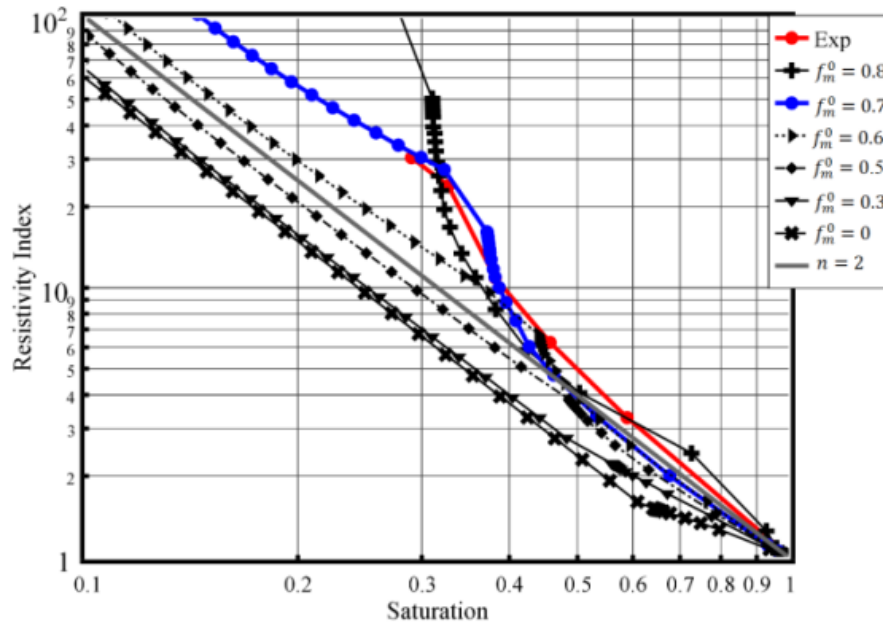


Figure 4-15: Effect of zero matrix porosity fractions

Figure 4-16 indicates the effect of changing the ratio R in the model of Estailades carbonate. The sharp increase in the curve is the effect of draining water from the corners of secondary pore space (vugs and throats). The throats have a significant effect, because they control the capillary pressure and, therefore the corner saturation when the secondary porosity is first invaded. A higher value of R signifies throats of greater side length and therefore a greater contribution to conductivity from water remaining in the corners following non-wetting phase invasion into the secondary pore spaces. Accordingly, RI becomes more sensitive to changes in water saturation as R increases, and effect more evident when parallel conduction pathways (conduction through matrix) are scarce.

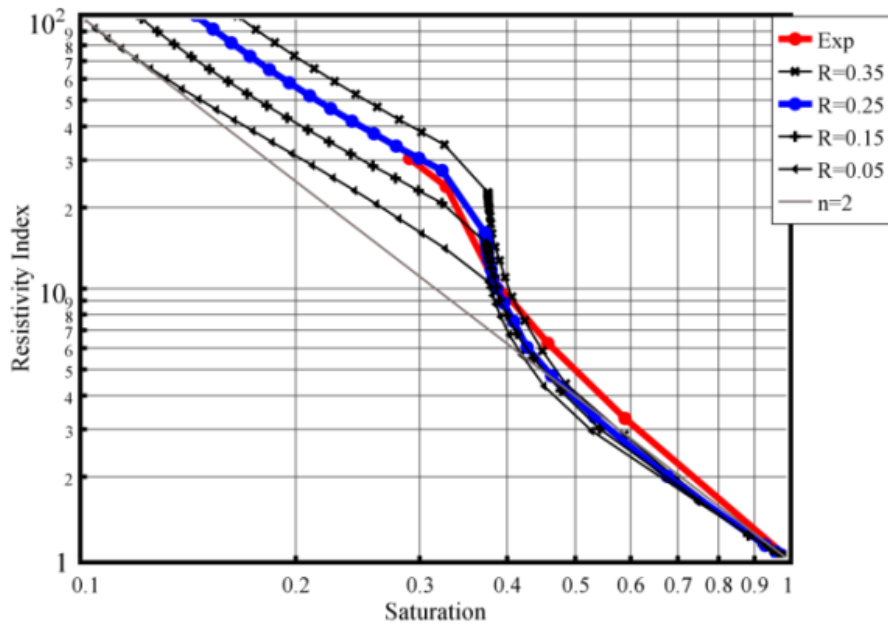


Figure 4-16: Effect of size ratio R

The effect of changing the connectivity exponent ω is depicted in Figure 4-17. ω is the parameter controlling the probability of communication of adjacent vugs via secondary pore space (vug throats), influencing significantly (albeit not exclusively) percolation of the secondary porosity. We compared the responses for three different values of ω . Two effects are observed as ω is increased from 0.7 to 1. Firstly, small negative deviations from Archie's law are seen at high saturation, understood as weakening of the dependence of resistivity on total saturation as drainage of water from a more connected network of vugs takes place. This is followed by a strengthening of the dependence of D-PNM resistivity on water saturation over a saturation range when conduction is dependent on water in the corners of drained vugs. Such strengthening, manifested as a sharp increase in RI, is more pronounced when the vugs are mostly connected to each other.

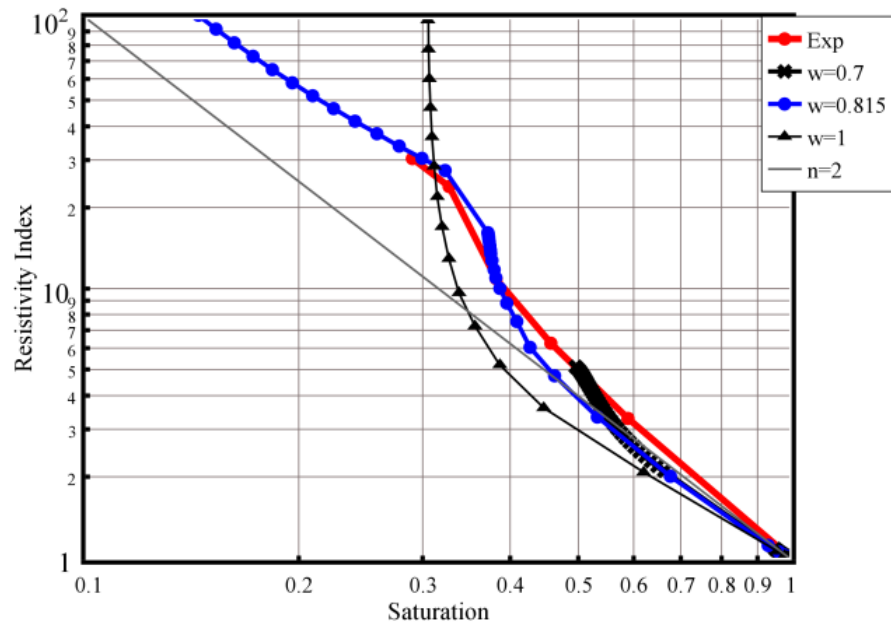


Figure 4-17: Effect of connectivity exponent

Figure 4-18 demonstrates a similar effect when the shape parameter of the distribution of secondary porosity is changed (see section 3.1.2.). Increasing the shape parameter decreases the skew of the vug side distribution, which increases the probability of connection between two adjacent vugs and thus shifts the RI curves to the left.

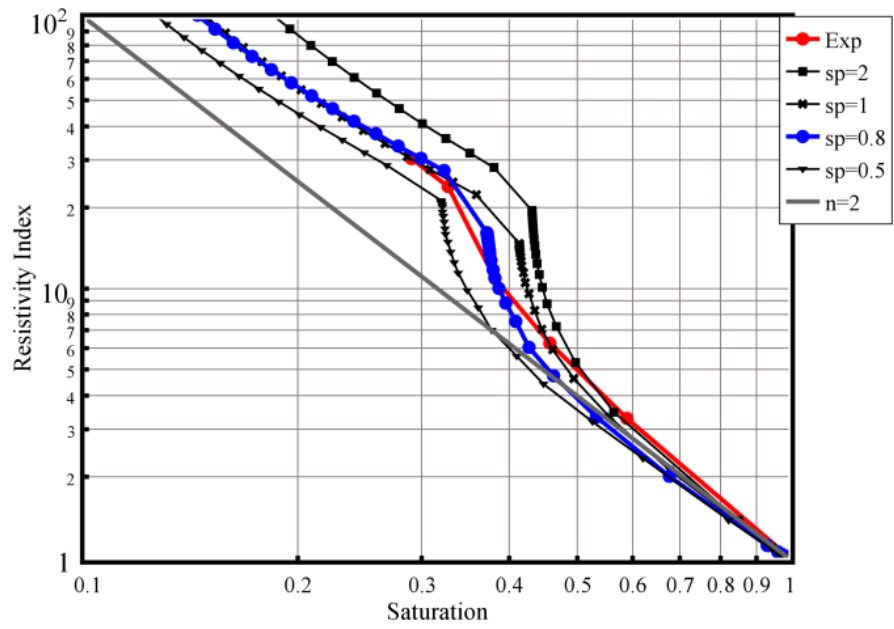


Figure 4-18: Effect of the shape of vug size distribution

Chapter 5

Conclusions

In this study, we have developed a realistic yet tractable dual pore network model (D-PNM) to relate electrical resistivity at partial saturation to key aspects of the pore structure of carbonate rocks. The model could be calibrated to the experimental data of the capillary pressure and electrical resistivity for two carbonate rock samples extensively studied in the literature. The D-PNM developed has to the following key features, all of which are important for the description of electrical resistivity: (1) it enables independent control of the connectivity and percolation of primary and secondary porosity, and thus accounts for the effects of fluid trapping, (2) it considers the effect of remaining fluid in the corners of drained secondary pores, (3) it can accommodate distribution and spatial structure of primary and secondary porosity. Specifically, the work presented in this thesis allows the following conclusions to be drawn from the data presented:

- The non-Archie behavior of bending down in the resistivity curve occurs even in one cell response. In a single cell, this behavior is associated with conduction via water in the corners of the secondary pore space.
- The D-PNM electrical responses have been classified into nine different types based on the degree of percolation and relative amount of matrix and secondary porosity. It is observed that the model is capable of stylistically reproducing all deviations from Archie's law.
- Non-Archie behavior of two different carbonate rocks (Estailades and Lavoux carbonates) has been modeled by the D-PNM in a manner consistent with experimental data from literature [17]. The properties of these two rocks (formation factor and total porosity) were consistent with the experimental data.

- Parametric studies have been conducted to explore the sensitivity of the D-PNM to key parameters: connectivity exponent, secondary porosity aspect ratio R , fraction of cells with zero matrix porosity and shape of vug size distribution. Model response is sensitive to all parameters considered. This indicates the potential to use the D-PNM for parameter estimation, using a minimum of petrophysical information (3D maps of porosity from microtomographic images and mercury intrusion capillary pressure data)
- Quantitative interpretation of the non-Archie behavior of the electrical resistivity of vuggy carbonates appears possible in the context of the D-PNM proposed, at a small fraction of the computational and information cost of alternative models attempting to reproduce in great detail the microstructure of carbonate rocks using microtomographic data.

Chapter 6

Recommendations

- The model has been verified for two different carbonate samples on the basis of electrical and capillary properties. The DPNM could be further interrogated for consistency (i) with other petrophysical properties, such as absolute and relative permeability and (ii) with experimental data for other carbonate rock samples.
- The model should be used for inverse modeling of experimental capillary pressure and electrical resistivity data for the purpose of best-fitting model parameters using an optimization approach conditioned on micro-tomographic data. This will relax the assumption of uniform matrix porosity and will enable incorporation of spatial structure of the secondary porosity, both of which are important aspects of heterogeneity.
- Water remaining in the corners of the secondary pore space has an important effect on electrical resistivity. This effect is presently taken into account by assuming simple corner geometry. A richer behavior would likely emerge if fractal geometry were to be considered. Further, modeling in this direction seems warranted.

Appendix A

Sample Appendix

The following is the programming code developed for simulating the D-PNM. It contains fourteen functions of MATLAB code.

(1) LBD

```
clc
clear all
tic
format longEng
% ***length of throat/length of vug***
R=.25;
% ***value of probability exponent***
w=0.815;
% ***length of each cell in meter***
L=0.0002;
%%***surface tension of water-air in N/m***
si=0.072;
Swr=0.02;
theita=0;
% ***Number of Network Cells***
i=1;
j=1;
k=1;
% ***Capillary Pressure Limit***
downlim=1;
uplim=60;
step=.2;
stepnum=(uplim-downlim)/step+1;
%Pmat=2^16;%8.7794*6.8948*10^3;%60532.2 in N/m^2 its about 2^16,
Breakthrough
D=Porosity(i,j,k);
Qv=D;
TotalPor=0;
A = zeros(i,j,k);
B = zeros(i,j,k);
Qs=zeros(i,j,k);
length=zeros(i*j*k,1);
Pc=1;
h=1;
p=1;
% ***Outputs***
counter=zeros(stepnum,5);
RIX=zeros(stepnum,1);
SAT=zeros(stepnum,1);
CAP=zeros(stepnum,1);
AccessibleCells=zeros(i,j,k);
[Qm,Pcbtm,PermeabilityTot]=MatrixPorosity(i,j,k);
```

```

for x=1:i
    for y=1:j
        for z=1:k
            Q=D(x,y,z);
            Prs(h,1)=Q;
            A(x,y,z)= NR(Q,R,L);
            length(h,1)=A(x,y,z);
            B(x,y,z)=R*A(x,y,z);%in meter
            h=h+1;
        end
    end
end
end
%hist(Prs)
%xlswrite('filemm',length)
%disp(A)
%disp(B)
%***Finding the Toatal Porosity of Network***
for x=1:i
    for y=1:j
        for z=1:k
            Qs(x,y,z)=(Qv(x,y,z)*(1-Qm(x,y,z)))+Qm(x,y,z);
            TotalPor=Qs(x,y,z)+TotalPor;
        end
    end
end
end
[ ms,FF ] = mfactor(
i,j,k,A,Pc,Pcbtm,Qm,R,Swr,si,theita,L,AccessibleCells,TotalPor);
%display(Qs)
% ***Get the Inlet Surface from the User***
[NCI,NCJ,NCK]=PCONNECTION(w,D,i,j,k);
M=input('Please Enter the Inlet Surface:x, y or z:','s');
% ***Finding the Total Saturation of Network***
for t=downlim:step:uplim%log2 of input capillary pressue(2^9<Pcbtv<2^12,
Pcbtm=2^16)
    %disp(t)
    Pc=2^t;
    [Pcbt,opcell,nvug,nmat]=OPCELL(Pcbtm,B,Pc,i,j,k,theita,si);
    lbd=opcell;
    % ***show the open cells with the cappillary pressure***
    %OPCEL(X), X is cappillary pressure in N/m^2
    [AccessibleCells,numac]=ACCESS(lbd,NCI,NCJ,NCK,M,Pc);
    counter(p,1)=Pc;
    counter(p,2)=i*j*k;
    counter(p,3)=nvug;
    counter(p,4)=nmat;
    counter(p,5)=numac;
    [RI,ROs]=RENORM(i,j,k,A,Pc,Pcbtm,Qm,R,Swr,si,theita,L,AccessibleCells);
    SatCell=zeros(i,j,k);
    SigmaSat=0;
    SatC=CellSat(Pcbtm,Qm,Qs,Swr,si,theita,L,A,B,D,Pc,i,j,k,AccessibleCells );
    for x=1:i
        for y=1:j
            for z=1:k

```

```

        SatCell(x,y,z)=SatC(x,y,z).*Qs(x,y,z);
        SigmaSat=SatCell(x,y,z)+SigmaSat;
    end
end
end
%display(SatCell)
%display(SigmaSat)
TotalSat=1-(SigmaSat/TotalPor);
PorosityTotal=TotalPor/(i*j*k);
subplot(3,1,1);
loglog(TotalSat,RI,'r*')
%hold on
%subplot(2,1,2);loglog(TotalSat,Pc,'m+')
RIX(p,1)=RI;
SAT(p,1)=TotalSat;
CAP(p,1)=Pc;
p=p+1;
hold on
end
hold on
% subplot(2,1,1)
% plot(log(CAP),1-SAT,'*');
hold on
[yint,dyint,xx,DIAMS]=xxsplines( CAP,SAT,si,theita );
xx=xx';
toc

```

(2) Matrix Porosity

```

function [ Qm,Pcbtm,PermeabilityTot ] = MatrixPorosity( i,j,k)
r=rand(i,j,k);
m=0;
n=0;
qq=0.3;
Pcbtm = zeros(i,j,k);
Perm = zeros(i,j,k);
TotalPerm=0;
for x=1:i
    for y=1:j
        for z=1:k
            if r(x,y,z)<=0.7
                m=m+1;
                r(x,y,z)=qq.*(10^-20);
            end
            if r(x,y,z)>0.7
                n=n+1;
                r(x,y,z)=qq;
            end
            Perm(x,y,z)=1859.3*(r(x,y,z).^1.732);
            TotalPerm=TotalPerm+Perm(x,y,z);%mDarcy
            Pcbtm(x,y,z)=20*6.8948*10^3*(12.6991)*(Perm(x,y,z).^(-0.369));
        end
    end
end
end

```

```

Qm=r;
PermeabilityTot=TotalPerm/(i*j*k);
end

```

(3) NR

```

function [ a ] = NR( Q ,R,L)
%***This function calculate a side lenght of cubic vug a(x)
%by using Q(vug porosity), R(b/a) and L(size of block)
%as a given value***
%L=0.01;%in meter
X(1)=Q;
E(1)=1;
i=1;
j=1;
%Newton-Raphson
while E(i)>.000005;
    i=i+1;
    X(i)=X(i-1)-((1-3*R^2).*X(i-1).^3+3*R^2.*X(i-1).^2-Q)/...
        (3*(1-3*R^2).*X(i-1).^2+6*R^2.*X(i-1));
    E(i)=abs((X(i)-X(i-1))/X(i));
    j=j+1;
    k=0;
    if j>50
        k=1;
        error('FAIL TO CONVERGE')
        break
    end
    if k==0;
a=X(i)*L;
    end
end
end

```

(4) MFACTOR

```

function [ ms,FF ] = mfactor(
i,j,k,A,Pc,Pcbtm,Qm,R,Swr,si,theita,L,AccessibleCells>TotalPor)
%***Calculating the formation factor***
%F=Qs^-ms
%F=RDPN(%100)/RWater
ro=20;%ohm-meter
Rwater=ro*(j*L)/((i*L)*(k*L));
[ ~,ROs ] = RENORM(i,j,k,A,Pc,Pcbtm,Qm,R,Swr,si,theita,L,AccessibleCells);
FF=ROs/Rwater;
QS=TotalPor/(i*j*k);
ms=-log(FF)/log(QS);
end

```

(5) Pconnection

```

function [ NCI,NCJ,NCK ] = PCONNECTION(w,D,i,j,k)
%***Probability of finding connection between two neighbouring blocks***
%w=0.7; %value of probability exponent

```

```

A=i;
B=j;
C=k;
%prosity network
%D=Porosity(A,B,C);
%making first column and first row zero
newD=zeros(A+1,B+1,C+1);
for a=1:A
for b=1:B
for c=1:C
    newD(a+1,b+1,c+1)=D(a,b,c);
end
end
end
D=newD;
A=A+1;
B=B+1;
C=C+1;
AA=zeros(A,B,C);
BB=zeros(A,B,C);
CC=zeros(A,B,C);
for x=2:A
    AA(x, :, :)=(D(x, :, :).*D(x-1, :, :)).^( (1-w)/w );
end
for y=2:B
    BB(:, y, :)=(D(:, y, :).*D(:, y-1, :)).^( (1-w)/w );
end
for z=2:C
    CC(:, :, z)=(D(:, :, z).*D(:, :, z-1)).^( (1-w)/w );
end

for x=2:A
for y=2:B
for z=2:C
if AA(x,y,z)>rand
    AA(x,y,z)=1;
else
    AA(x,y,z)=0;
end

if BB(x,y,z)>rand
    BB(x,y,z)=1;
else
    BB(x,y,z)=0;
end

if CC(x,y,z)>rand
    CC(x,y,z)=1;
else
    CC(x,y,z)=0;
end
end
end
end

```

```

end
NCI=AA;%above
NCJ=BB;%left
NCK=CC;%inside
end

```

(6) OPCELL

```

function [Pcbt,opcell,nvug,nmat] = OPCELL(Pcbtm,B,Pc,i,j,k,theita,si)
openpres=Pc;%in N/m^2
%***Finding the constant dimensionless Pc prime***
%theita=0;
lambda=1;
nvug=0;
nmat=0;
%si=0.072;%surface tension of water-air in N/m
F1=((pi/2)-(2*theita))-(2*sqrt(2)*cos(theita)*sin((pi/4)-theita));
F2=(0.5*sin((pi/2)-2*theita))+((sin((pi/4)-theita))^2)-((pi/4)-theita);
%a=F1*F2;
%b=2*(lambda+1)*F2*cos(theita);
%c=lambda*F1;
%P=[a b c];
%Rprime=min(roots(P));
Rprime=0.5302;
Pcp=((lambda+1)*cos(theita)+(Rprime*F1))/(lambda-(Rprime^2*F2));
Pcbt = zeros(i,j,k);
opcell=zeros(i,j,k);
%***Finding the Breakthroughthrough Capillary Pressure for Each Cell***
%disp(D)
%pres=zeros(i*j*k,1);
for x=1:i;
for y=1:j;
for z=1:k
Pcbt(x,y,z)=(Pcp*si^2)/B(x,y,z);%in N/m^2
if (openpres > Pcbt(x,y,z) )&&(openpres<Pcbtm(x,y,z))
opcell(x,y,z)=1;
nvug=nvug+1;
elseif openpres > Pcbtm(x,y,z)
opcell(x,y,z)=2;
nmat=nmat+1;
end
%hist(log2(Pcbt))
%set(gca,'XScale','log2')
%plot(Pcapmx,0,'*')
end
end
end
end
end

```

(7) ACCESS

```

function [ ACS,numac ] = ACCESS(lbd,NCI,NCJ,NCK,M,Pc )
%***Finding the Accessible Clusters***

```

```

%disp(D)
numac=0;
[cls]=SK(lbd,NCI,NCJ,NCK);
[p, q, r]=size(lbd);
if M=='x'
    n=q*r;
    N=zeros(1,n);
    k=1;
    for b=1:q
        for c=1:r
            if cls(1,b,c)~=0
                N(1,k)=cls(1,b,c);
                M=zeros(1,k);
            end
        end
    end
    for m=1:k
        M(1,m)=N(1,m);
    end
    k=k+1;
end
end
end
end
for a=2:p
    for b=1:q
        for c=1:r
            if cls(a,b,c)~=0
                if any(M==cls(a,b,c))==0
                    cls(a,b,c)=0;
                end
            end
        end
    end
end
end
s=0;
for b=1:q
    for c=1:r
        if s==0
            if cls(p,b,c)~=0
                if any(M==cls(p,b,c))~=0
                    % disp('Percolation')
                    % disp(Pc)
                    s=1;
                end
            end
        end
    end
end
end
elseif M=='y'
    n=p*r;
    N=zeros(1,n);
    k=1;
    for a=1:p
        for c=1:r
            if cls(a,1,c)~=0
                N(1,k)=cls(a,1,c);
            end
        end
    end
end

```

```

        M=zeros(1,k);
for m=1:k
    M(1,m)=N(1,m);
end
    k=k+1;
    end
    end
    end
for a=1:p
for b=2:q
for c=1:r
if cls(a,b,c)~=0
if any(M==cls(a,b,c))==0
    cls(a,b,c)=0;
end
end
end
end
end
s=0;
for a=1:p
for c=1:r
    if s==0
if cls(a,q,c)~=0
if any(M==cls(a,q,c))~=0
    %disp('Percolation')
    %disp(Pc)
    s=1;
end
end
        end
    end
end
elseif M=='z'
    n=p*q;
    N=zeros(1,n);
    k=1;
    for a=1:p
        for b=1:q
            if cls(a,b,1)~=0
                N(1,k)=cls(a,b,1);
                M=zeros(1,k);
            end
        end
    end
for m=1:k
    M(1,m)=N(1,m);
end
    numac=k;
    k=k+1;

    end
    end
    end
for a=1:p
for b=1:q

```



```

        R2=Rcell(x,y+1,z);
        R3=Rcell(x+1,y,z);
        R4=Rcell(x+1,y+1,z);
        R5=Rcell(x,y,z+1);
        R6=Rcell(x,y+1,z+1);
        R7=Rcell(x+1,y,z+1);
        R8=Rcell(x+1,y+1,z+1);
        RoutKirch= Kirchhoffs(R1,R2,R3,R4,R5,R6,R7,R8);
        R(x,y,z)=RoutKirch/2;
    end
end
end
R0((1:i/2),(1:j/2),(1:k/2))=R0(1:2:x,1:2:y,1:2:z);
Rcell((1:i/2),(1:j/2),(1:k/2))=R(1:2:x,1:2:y,1:2:z);
R0=R0(1:i/2,1:j/2,1:k/2);
Rcell=Rcell(1:i/2,1:j/2,1:k/2);
i=i/2;j=j/2;k=k/2;
p=i;
end
RI=Rcell/R0;
R0s=R0*2;
%disp(RI)
end

```

(9) CELLSAT

```

function [ Snw] =
CellSat(Pcbtn,Qm,Qs,Swr,si,theita,L,A,B,D,Pc,i,j,k,AccessibleCells )
[Pcbtn,opcell]=OPCELL(Pcbtn,B,Pc,i,j,k,si,theita);
Qv=D;
Snw=ones(i,j,k);
Pcprime=zeros(i,j,k);
Rprime=zeros(i,j,k);
Vcol=zeros(i,j,k);
Vco2=zeros(i,j,k);
Vco=zeros(i,j,k);
Vthroat=zeros(i,j,k);
Satvug=zeros(i,j,k);
Smnw=zeros(i,j,k);
%***Matrix Saturation***
for x=1:i
    for y=1:j
        for z=1:k
            if Pc>Pcbtn(x,y,z)
                if AccessibleCells(x,y,z)~=0
                    Pstar=Pc./Pcbtn(x,y,z);
                    Sweff=Pstar^(-0.6666);
                    Smw=(Sweff*(1-Swr))+Swr;%each cell matrix saturation
                    Smnw(x,y,z)=1-Smw;%nonwetting phase sat
                    Pcprime(x,y,z)=(Pc*B(x,y,z))/(2*si);
                    Rprime(x,y,z)=1/Pcprime(x,y,z);
                    F2=(0.5*sin((pi/2)-2*theita))+((sin((pi/4)-theita))^2)-
((pi/4)-theita);

```

```

                %Find the non occupied volume
                Vcol(x,y,z)=( (B(x,y,z)/2) .*Rprime(x,y,z) ).^2.*( (L-
A(x,y,z) )/2) *F2*24;

Vco2(x,y,z)=( (A(x,y,z)/2) .*Rprime(x,y,z) ).^2.*A(x,y,z) *F2*8;
                Vco(x,y,z)=Vcol(x,y,z)+Vco2(x,y,z);
                Vthroat(x,y,z)=(6*(B(x,y,z).^2) .* ( (L-
A(x,y,z) )/2) )+A(x,y,z).^3;
                Satvug(x,y,z)=1-(Vco(x,y,z)/Vthroat(x,y,z));
                end
            end

***Vug Saturation***
            if (Pc>Pcibt(x,y,z) ) && (Pc<Pcibtm(x,y,z) )
                if AccessibleCells(x,y,z) ~ =0
                    Pcprime(x,y,z)=(Pc*B(x,y,z) ) / (2*si);
                    Rprime(x,y,z)=1/Pcprime(x,y,z);
                    F2=(0.5*sin((pi/2)-2*theita) )+((sin((pi/4)-theita) )^2)-((pi/4)-
theita);
                    %Find the non occupied volume
                    Vcol(x,y,z)=( (B(x,y,z)/2) .*Rprime(x,y,z) ).^2.*( (L-
A(x,y,z) )/2) *F2*24;
                    Vco2(x,y,z)=( (A(x,y,z)/2) .*Rprime(x,y,z) ).^2.*A(x,y,z) *F2*8;
                    Vco(x,y,z)=Vcol(x,y,z)+Vco2(x,y,z);
                    Vthroat(x,y,z)=(6*(B(x,y,z).^2) .* ( (L-A(x,y,z) )/2) )+A(x,y,z).^3;
                    Satvug(x,y,z)=1-(Vco(x,y,z)/Vthroat(x,y,z));
                end
            end

***each cell saturation***
            Snw(x,y,z)=( (Qv(x,y,z) .*Satvug(x,y,z) )+((1-
Qv(x,y,z) ) .*Qm(x,y,z) .*Smnw(x,y,z) ) ) ...
            ./Qs(x,y,z);
            end
        end
    end
    %Qss=Qs
    %MatrixSaturation=Smw;
    %VugSaturation=Satvug
    %Satcell=Sw
end

```

(10) CELLRESIS

```

function[Rcell,R0]=CellResis(i,j,k,A,Pc,Pcibt,Qm,R,Swr,si,theita,L,Accessi
bleCells)
ro=20;%ohm-meter
m=2;
n=2;
Pcp=1.8862;
F2=(0.5*sin((pi/2)-2*theita) )+((sin((pi/4)-theita) )^2)-((pi/4)-theita);
Pcibt=zeros(i,j,k);
Rvug=zeros(i,j,k);

```

```

Rmatrix=zeros(i,j,k);
Rcell=zeros(i,j,k);
R0vug=zeros(i,j,k);
R0matrix=zeros(i,j,k);
R0=zeros(i,j,k);
Rprime=zeros(i,j,k);
Pcprime=zeros(i,j,k);
B=R.*A;
for x=1:i
    for y=1:j
        for z=1:k
            Pcbt(x,y,z)=(Pcp*si*2)/B(x,y,z);
            R0vug(x,y,z)=(ro/2)*((L-A(x,y,z))/B(x,y,z).^2+(1/A(x,y,z)));
            Rvug(x,y,z)=R0vug(x,y,z);
            R0matrix(x,y,z)=(ro/2)*((L-A(x,y,z))./(L^2)-
(B(x,y,z).^2))+...
            (A(x,y,z)./(L^2)-(A(x,y,z).^2))) *Qm(x,y,z).^-m;
            Rmatrix(x,y,z)=R0matrix(x,y,z);
            if Pc>Pcbtm(x,y,z)
                if AccessibleCells(x,y,z)~=0
                    Pstar=Pc./Pcbtm(x,y,z);
                    Sweff=Pstar^(-0.6666);
                    Smw=(Sweff*(1-Swr))+Swr;%each cell matrix saturation water
                    Rmatrix(x,y,z)=(ro/2)*((L-A(x,y,z))/(L^2)-
(B(x,y,z).^2))+...
                    (A(x,y,z)/(L^2)-(A(x,y,z).^2))).*Smw^-n*Qm(x,y,z).^-
m;

                    Pcprime(x,y,z)=(Pc*B(x,y,z))/(2*si);
                    Rprime(x,y,z)=1/Pcprime(x,y,z);
                    At=((B(x,y,z)/2).*Rprime(x,y,z)).^2)*F2*4;
                    Av=((A(x,y,z)/2).*Rprime(x,y,z)).^2)*F2*4;
                    Rvug(x,y,z)=(ro/2)*((L-A(x,y,z))/At)+(A(x,y,z)/Av);
                    end
                end
            if (Pc>Pcbt(x,y,z)) && (Pc<Pcbtm(x,y,z))
                if AccessibleCells(x,y,z)~=0
                    Pcprime(x,y,z)=(Pc*B(x,y,z))/(2*si);
                    Rprime(x,y,z)=1/Pcprime(x,y,z);
                    At=((B(x,y,z)/2).*Rprime(x,y,z)).^2)*F2*4;
                    Av=((A(x,y,z)/2).*Rprime(x,y,z)).^2)*F2*4;
                    Rvug(x,y,z)=(ro/2)*((L-A(x,y,z))/At)+(A(x,y,z)/Av);
                    end
                end
            if A(x,y,z)==0
                Rcell(x,y,z)=Rmatrix(x,y,z);
                R0(x,y,z)=R0matrix(x,y,z);
            else
                Rcell(x,y,z)= 1/((1/(Rvug(x,y,z)))+(1/Rmatrix(x,y,z)));
                R0(x,y,z)=1/((1/(R0vug(x,y,z)))+(1/R0matrix(x,y,z)));
            end
            %RI(x,y,z)=Rcell(x,y,z);%R0(x,y,z);
        end
    end
end

```

```

end
%display(R0)
%display(Rcell)
end

```

(11) KIRSHOF

```

function [ RoutKirch ] = Kirchhoffs(R1,R2,R3,R4,R5,R6,R7,R8)
%This fuction get 8 resistivity as an input and simplify it to one resis
%by using renormalization method
%***step1***

%left side
A=R3;
B=R1;
C=R5;
D=R7;
%right side
E=R4;
F=R2;
G=R6;
H=R8;
%center cubic
%outside
I=R1+R3;
J=R1+R2;
K=R2+R4;
L=R3+R4;
%inside
M=R5+R7;
N=R5+R6;
O=R6+R8;
P=R7+R8;
%side
Q=R1+R5;
R=R3+R7;
S=R2+R6;
T=R4+R8;
%LU Factorization Method
a=[1/J+1/I+1/B+1/Q -1/J -1/I 0 -1/Q 0 0 0;
-1/J 1/J+1/K+1/F+1/S 0 -1/K 0 -1/S 0 0;
-1/I 0 1/I+1/L+1/A+1/R -1/L 0 0 -1/R 0;
0 -1/K -1/L 1/K+1/L+1/T+1/E 0 0 0 -1/T;
-1/Q 0 0 0 1/Q+1/N+1/M+1/C -1/N -1/M 0;
0 -1/S 0 0 -1/N 1/S+1/N+1/O+1/G 0 -1/O;
0 0 -1/R 0 -1/M 0 1/D+1/R+1/M+1/P -1/P;
0 0 0 -1/T 0 -1/O -1/P 1/T+1/O+1/P+1/H];
b=[1/B;0;1/A;0;1/C;0;1/D;0];
%Y=linsolve(a,b)
V=mldivide(a,b);
I2=V(2)/F;
I4=V(4)/E;
I6=V(6)/G;

```

```

I8=V(8)/H;
I=I2+I4+I6+I8;
%I1=(1-V(1))/B;
%I3=(1-V(3))/A;
%I5=(1-V(5))/C;
%I7=(1-V(7))/D;
%Iplus=I1+I3+I5+I7;
RoutKirch=1/I;
end

```

(12) SK

```

function [ cls ] =SK(lbd,NCI,NCJ,NCK)
%***Hoshen & Kopelman algorithm with considering the probability of
%connections***
%Probability of finding connection between two neighbouring blocks
[i, j, k]=size(lbd);
newlabel=0;
cntr=1;
%making first column and first row zero
newlbd=zeros(i+1,j+1,k+1);
for a=1:i
for b=1:j
for c=1:k
newlbd(a+1,b+1,c+1)=lbd(a,b,c);
end
end
end
lbd=newlbd;
i=i+1;
j=j+1;
k=k+1;
%define cluster size array
q=i*j*k;
csize=zeros(q,1);
%Matrix traverse
for z=2:k
for x=2:i
for y=2:j
if lbd(x,y,z)==2
lbdx=lbd(x-1,y,z);
lbdy=lbd(x,y-1,z);
lbdz=lbd(x,y,z-1);
if lbdx==2
NCI(x,y,z)=1;
end
if lbdy==2
NCJ(x,y,z)=1;
end
if lbdz==2
NCK(x,y,z)=1;
end
end
end
end
end
end

```

```

    end
end
for z=2:k
    for x=2:i
        for y=2:j
            if lbd(x,y,z)==2
                lbd(x,y,z)=1;
            end
        end
    end
end

for z=2:k
    for x=2:i
        for y=2:j
            if lbd(x,y,z)~=0
                lbdx=lbd(x-1,y,z);
                lbdy=lbd(x,y-1,z);
                lbdz=lbd(x,y,z-1);
                above=lbdx*NCI(x,y,z);
                left=lbdy*NCJ(x,y,z);
                inside=lbdz*NCK(x,y,z);
                if (above~=0)&&(left~=0)&&(inside~=0)
                    if above==left==inside
                        lbd(x,y,z)=above;
                        if csize(above,1)>0
                            csize(above,1)=csize(above,1)+1;
                        end
                    else
                        mn1=min(above,left);
                        mn2=min(above,inside);
                        mx1=max(above,left);
                        mx2=max(above,inside);
                        mn=min(mn1,mn2);
                        avg=max(mn1,mn2);
                        mx=max(mx1,mx2);
                        lbd(x,y,z)=mn;
                        if csize(mn,1)>0
                            csize(mn,1)=csize(mn,1)+1;
                        end
                        s=csize(mx,1);
                        csize(mx,1)=-mn;
                        if s<0
                            n=1;
                            while n<1000
                                if s<0
                                    v=abs(s);
                                    s=csize(abs(s),1);
                                    csize(v,1)=-mn;
                                    n=n+1;
                                elseif s>0
                                    break;
                                end
                            end
                        end
                    end
                end
            end
        end
    end
end

```

```

        end
    end
    s=csize(avg,1);
    csize(avg,1)=-mn;
    if s<0
        n=1;
        while n<1000
            if s<0
                v=abs(s);
                s=csize(abs(s),1);
                csize(v,1)=-mn;
                n=n+1;
            elseif s>0
                break;
            end
        end
    end
end
elseif (above~=0) && (left==0) && (inside==0)
    lbd(x,y,z)=above;
    if csize(above,1)>0
        csize(above,1)=csize(above,1)+1;
    end
elseif (above==0) && (left~=0) && (inside==0)
    lbd(x,y,z)=left;
    if csize(left,1)>0
        csize(left,1)=csize(left,1)+1;
    end
elseif (above==0) && (left==0) && (inside~=0)
    lbd(x,y,z)=inside;
    if csize(inside,1)>0
        csize(inside,1)=csize(inside,1)+1;
    end
elseif (above~=0) && (left~=0) && (inside==0)
    mn=min(above,left);
    mx=max(above,left);
    lbd(x,y,z)=mn;
    if csize(mn,1)>0
        csize(mn,1)=csize(mn,1)+1;
    end
    s=csize(mx,1);
    csize(mx,1)=-mn;
    if s<0
        n=1;
        while n<1000
            if s<0
                v=abs(s);
                s=csize(abs(s),1);
                csize(v,1)=-mn;
                n=n+1;
            elseif s>0
                break;
            end
        end
    end
end

```

```

        end
    end
elseif (above==0) && (left~=0) && (inside~=0)
    mn=min(left,inside);
    mx=max(left,inside);
    lbd(x,y,z)=mn;
    if csize(mn,1)>0
        csize(mn,1)=csize(mn,1)+1;
    end
    s=csize(mx,1);
    csize(mx,1)=-mn;
    if s<0
        n=1;
        while n<1000
            if s<0
                v=abs(s);
                s=csize(abs(s),1);
                csize(v,1)=-mn;
                n=n+1;
            elseif s>0
                break;
            end
        end
    end
elseif (above~=0) && (left==0) && (inside~=0)
    mn=min(above,inside);
    mx=max(above,inside);
    lbd(x,y,z)=mn;
    if csize(mn,1)>0
        csize(mn,1)=csize(mn,1)+1;
    end
    s=csize(mx,1);
    csize(mx,1)=-mn;
    if s<0
        n=1;
        while n<1000
            if s<0
                v=abs(s);
                s=csize(abs(s),1);
                csize(v,1)=-mn;
                n=n+1;
            elseif s>0
                break;
            end
        end
    end
else
    newlabel=newlabel+1;
    lbd(x,y,z)=newlabel;
    csize(newlabel,1)=cntr;
end
end
end
end

```

```

    end
end
%display(lbd)
%display(csize)
%check the csize of clusters
for z=2:k
    for x=2:i
        for y=2:j
            if lbd(x,y,z)~=0
                d=csize(lbd(x,y,z),1);
                if d<0
                    m=1;
                    while m<1000
                        if d<0
                            e=abs(d);
                            d=csize(abs(d),1);
                            if e==abs(d)
                                lbd(x,y,z)=e;
                            end
                            m=m+1;
                        elseif d>0
                            lbd(x,y,z)=e;
                        break;
                    end
                end
            end
        end
    end
end
end
end
new2lbd=zeros(i-1,j-1,k-1);
for a=2:i
    for b=2:j
        for c=2:k
            new2lbd(a-1,b-1,c-1)=lbd(a,b,c);
        end
    end
end
cls=new2lbd;
end

```

(13) TRIDIAG

```

function x = Tridiag(e,f,g,r)
% x = Tridiag(e,f,g,r):
%   Tridiagonal system solver.
% input:
%   e = subdiagonal vector
%   f = diagonal vector
%   g = superdiagonal vector
%   r = right hand side vector
% output:
%   x = solution vector
n=length(f);

```

```

% forward elimination
for k = 2:n
    factor = e(k)/f(k-1);
    f(k) = f(k) - factor*g(k-1);
    r(k) = r(k) - factor*r(k-1);
end
% back substitution
x(n) = r(n)/f(n);
for k =n-1:-1:1
    x(k) = (r(k)-g(k)*x(k+1))/f(k);
end

```

(14) XXSPLINES

```

function [ yint,dyint,xx,DIAMS] = xxsplines(CAP,SAT,si,theita)
%function yint = mysplines(x,y,xx)
DIAMS = (10^6)*4*si*cos(theita)./CAP;
x=flipud(log10(DIAMS));
y=flipud(1-SAT);

nsplines = length(x)-1;%Number of cubic splines to be determined

for i = 1:nsplines
    h(i) = x(i+1)-x(i);
    d(i) = y(i);
end

iknots = nsplines -1; %Number of internal knots

%Set up the tridiagonal system of equations
e(1) = 0;
g(iknots)=0;
for i = 2:iknots
    e(i) = h(i);
end
for i = 1:iknots
    f(i) = 2*(h(i)+h(i+1));
    r(i) = 6*((y(i+2)-y(i+1))/h(i+1)-(y(i+1)-y(i))/h(i));
end
for i = 1:iknots-1
    g(i) = h(i+1);
end

%Solve the tridiagonal system to get second derivative at the internal
%knots
sol = Tridiag(e,f,g,r);

S=zeros(nsplines+1, 1);

for i = 2:nsplines
    S(i) = sol(i-1);
end

```

```

for i = 1:nsplines
    b(i) = S(i)/2;
    a(i) = (S(i+1)-S(i))/(6*h(i));
    c(i) = (y(i+1)-y(i))/h(i) - (2*h(i)*S(i)+h(i)*S(i+1))/6;
end

%Use cubic splines to interpolate

xx = (min(x)+1):.1:(max(x)-1);
yint = zeros(length(xx),1);
dyint=zeros(length(xx),1);

for j = 1:length(xx) %for each xx where interpolation is needed
    found = 0; %Variable to indicate when proper spline has been
found
    i = 1;
    while found==0 %Search for the interval containing xx to locate
proper spline
        if x(i)<=xx(j) && xx(j)<=x(i+1)
            yint(j) = a(i)*(xx(j)-x(i))^3+b(i)*(xx(j)-x(i))^2+...
                c(i)*(xx(j)-x(i))+d(i);
            dyint(j) = 3*a(i)*(xx(j)-x(i))^2+2*b(i)*(xx(j)-x(i))+c(i);
            found = 1;
        else
            i = i+1;
        end
    end
end

subplot(3,1,2)
plot(x,y,'ro',xx,yint);
subplot(3,1,3)
plot(xx,dyint)
end

```

Bibliography

- [1] Schlumberger, “Schlumberger Market Analysis,” 2007. [Online]. Available: <http://www.slb.com/>.
- [2] G. Archie, “The Electrical Resistivity Log as an Aid in Determining Some Reservoir Characteristics,” *Pet. Trans. AIME*, vol. 146, pp. 54–62, 1942.
- [3] J. R. Dixon and B. F. Marek, “The Effect of Bimodal Pore Size Distribution on Electrical Properties of Some Middle Eastern Limestones,” *Soc. Pet. Eng. 20601*, pp. 743–750, Apr. 1990.
- [4] J. W. Focke and D. Munn, “Cementation Exponents in Middle Eastern Carbonate Reservoirs,” *Soc. Pet. Eng. 13735*, pp. 155–167, 1985.
- [5] S. Saner, A. Al-Harathi, and M. T. Htay, “Use of Tortuosity for Discriminating Electro-facies to Interpret the Electrical Parameters of Carbonate Reservoir Rocks,” *J. Pet. Sci. Eng.*, vol. 16, no. 4, pp. 237–249, Dec. 1996.
- [6] M. Fleury, “Resistivity in Carbonates: New Insights,” *Proc. SPE Annu. Tech. Conf. Exhib.*, pp. 1–12, Sep. 2002.
- [7] G. S. Padhy, M. A. Ioannidis, C. Lemaire, and M. Coniglio, “Measurement and Interpretation of Non-Archie Resistivity Behavior in Model and Real Vuggy Carbonates,” *Soc. Core Anal.*, vol. 11, pp. 1–11, 2006.
- [8] M. J. Petricola and M. Walf, “Effect of Microporosity in Carbonates: Introduction of a Versatile Saturation Equation,” *Soc. Pet. Eng.*, pp. 607–615, 1995.
- [9] A. I. M. Dicker and W. A. Bemelmans, “Models for Simulating the Electrical Resistance of Porous Media,” *SPWLA 25th Annu. Logging Symp.*, pp. 1–12, 1984.
- [10] M. Han, M. Fleury, and P. Levitz, “Effect of the Pore Structure on Resistivity Index Curves,” *Soc. Core Anal.*, vol. 34, no. 1997, pp. 1–12, 2007.
- [11] P. N. Sen, “Resistivity of Partially Saturated Carbonate Rocks with Microporosity,” *Geophysics*, vol. 62, no. 2, pp. 415–425, 1997.
- [12] M. A. Ioannidis, M. J. Kwiecien, and I. Chatzis, “Electrical Conductivity and Percolation Aspects of Statistically Homogeneous Porous Media,” *Transp. Porous Media*, vol. 29, pp. 61–83, 1997.
- [13] B. Montaron, “Connectivity Theory – A New Approach to Modeling Non-Archie Rocks,” *Petrophysics*, vol. 50, no. 2, 2009.

- [14] D. Zhou, S. Arbabi, and E. H. Stenby, "A Percolation Study of Wettability Effect on the Electrical Properties of Reservoir Rocks," *Transp. Porous Media*, vol. 29, no. 1, pp. 85–98, 1997.
- [15] G. S. Padhy, M. A. Ioannidis, and C. Lemaire, "Interpretation of the Non-Archie Resistivity Behaviour in Vuggy Carbonates: Use of Pore Structure Parameters," *SPWLA Middle East Reg. Symp.*, pp. 1–14, 2007.
- [16] M. Han, S. Youssef, E. Rosenberg, M. Fleury, and P. Levitz, "The Effect of the Porous Structure on Resistivity Index Curves. an Experimental and Numerical Study.," *SPWLA 49th Annu. Logging Symp.*, pp. 1–10, 2008.
- [17] D. Bauer, S. Youssef, M. Han, S. Bekri, E. Rosenberg, M. Fleury, and O. Vizika, "From Computed Microtomography Images to Resistivity Index Calculations of Heterogeneous Carbonates Using a Dual-porosity Pore-network Approach: Influence of percolation on the electrical Transport Properties," *Phys. Rev. E*, vol. 84, no. 1, p. 011133, Jul. 2011.
- [18] M. A. Ioannidis and I. Chatzis, "A Dual-Network Model of Pore Structure for Vuggy Carbonates," *Proc. Annu. Symp. Soc. Core Anal.*, 2000.
- [19] F. L. Dullien, *Porous Media: Fluid Transport and Pore Structure*. Academic Press, 1991, p. 574.
- [20] M. A. Ioannidis, "On the Description of Capillary and Transport Phenomena in Heterogeneous Porous Media," University of Waterloo, Waterloo, Ontario, 1993.
- [21] R. Defay and I. Prigogine, *Surface Tension and Adsorption*. London: London: Longmans, 1966.
- [22] I. Chatzis, "A Network Approach to Analyze and Model Capillary and Transport Phenomena in Porous Media," University of Waterloo, 1980.
- [23] B. Legait, "Laminar Flow of Two Phases Through a Capillary Tube with Variable Square Cross-section," *J. Colloid Interface Sci.*, vol. 96, no. 1, pp. 28–38, Nov. 1983.
- [24] A. Y. Dandekar, *Petroleum Reservoir Rock and Fluid Properties*. CRC Press, 2013, p. 544.
- [25] J. Hoshen and R. Kopelman, "Percolation and cluster distribution. I. Cluster multiple labeling technique and critical concentration algorithm," *Phys. Rev. B*, vol. 14, no. 8, pp. 3438–3445, 1976.
- [26] M. L. Aldridge, "A Finite State Machine Approach to Cluster Identification Using the Hoshen-Kopelman Algorithm," The University of Tennessee, Knoxville, 2008.
- [27] M. A. Ioannidis and I. Chatzis, "Network Modeling of Pore Structure and Transport Properties of Porous Media," *Chem. Eng. Sci.*, vol. 48, no. 5, pp. 951–972, 1993.

- [28] Y. Nakashima and T. Nakano, "Accuracy of Formation Factors for Three-dimensional Pore-scale Images of Geo-materials Estimated by Renormalization Technique," *J. Appl. Geophys.*, vol. 75, no. 1, pp. 31–41, Sep. 2011.
- [29] P. R. King, "The Use of Renormalization for Calculating Effective Permeability," *Transp. Porous Media*, vol. 4, pp. 37–58, 1989.
- [30] D. Bauer, S. Youssef, M. Fleury, S. Bekri, E. Rosenberg, and O. Vizika, "Improving the Estimations of Petrophysical Transport Behavior of Carbonate Rocks Using a Dual Pore Network Approach Combined with Computed Microtomography," *Transp. Porous Media*, vol. 94, no. 2, pp. 505–524, Jan. 2012.